









Volcanic controls on the microbial habitability of Mars-analogue hydrothermal environments

Arola Moreras-Marti¹  | Mark Fox-Powell^{1,5}  | Aubrey L. Zerkle¹  |
 Eva Stueeken¹  | Fernando Gazquez²  | Helen E. A. Brand³  |
 Toni Galloway¹ | Lotta Purkamo⁴  | Claire R. Cousins¹ 

¹School of Earth and Environmental Sciences, University of St Andrews, St Andrews, UK

²Water Resources and Environmental Geology Research Group, Department of Biology and Geology, University of Almería, Almería, Spain

³Australian Synchrotron, Clayton, Vic., Australia

⁴Geological Survey of Finland, Espoo, Finland

⁵AstrobiologyOU, The Open University, Milton Keynes, UK

Correspondence

Arola Moreras-Marti, School of Earth and Environmental Sciences, University of St Andrews, Irvine Building, North Street, St Andrews, Fife, UK, KY16 9AL.
 Email: amm48@st-andrews.ac.uk

Funding information

UK Space Agency; Europlanet 2017 TA1 facility; Earth and Space Foundation; Orkustofnun

Abstract

Due to their potential to support chemolithotrophic life, relic hydrothermal systems on Mars are a key target for astrobiological exploration. We analysed water and sediments at six geothermal pools from the rhyolitic Kerlingarfjöll and basaltic Kverkfjöll volcanoes in Iceland, to investigate the localised controls on the habitability of these systems in terms of microbial community function. Our results show that host lithology plays a minor role in pool geochemistry and authigenic mineralogy, with the system geochemistry primarily controlled by deep volcanic processes. We find that by dictating pool water pH and redox conditions, deep volcanic processes are the primary control on microbial community structure and function, with water input from the proximal glacier acting as a secondary control by regulating pool temperatures. Kerlingarfjöll pools have reduced, circum-neutral CO₂-rich waters with authigenic calcite-, pyrite- and kaolinite-bearing sediments. The dominant metabolisms inferred from community profiles obtained by 16S rRNA gene sequencing are methanogenesis, respiration of sulphate and sulphur (S⁰) oxidation. In contrast, Kverkfjöll pools have oxidised, acidic (pH < 3) waters with high concentrations of SO₄²⁻ and high argillic alteration, resulting in Al-phyllsilicate-rich sediments. The prevailing metabolisms here are iron oxidation, sulphur oxidation and nitrification. Where analogous ice-fed hydrothermal systems existed on early Mars, similar volcanic processes would likely have controlled localised metabolic potential and thus habitability. Moreover, such systems offer several habitability advantages, including a localised source of metabolic redox pairs for chemolithotrophic microorganisms and accessible trace metals. Similar pools could have provided transient environments for life on Mars; when paired with surface or near-surface ice, these habitability niches could have persisted into the Amazonian. Additionally, they offer a confined site for biosignature formation and deposition that lends itself well to in situ robotic exploration.

KEYWORDS

analogue, hydrothermal systems, Iron, Mars, redox, sulfur

This is an open access article under the terms of the Creative Commons Attribution-NonCommercial License, which permits use, distribution and reproduction in any medium, provided the original work is properly cited and is not used for commercial purposes.

© 2021 The Authors. *Geobiology* published by John Wiley & Sons Ltd.

1 | INTRODUCTION

The Noachian period of Martian history (~4.1 to 3.7 Ga) was characterised by widespread volcanism and impact bombardment (Phillips et al., 2001; Segura et al., 2002). These events triggered localised hydrothermal activity within the Martian crust through interaction with Mars' hydro- or cryosphere, providing transient surface and subsurface heat, liquid water and geochemical energy (Schulze-Makuch et al., 2007). The combination of these factors could have provided localised habitats for chemotrophic microorganisms (Cockell & Lee, 2002; Osinski et al., 2013).

Likewise, within either 'warm' or 'cold' climatic scenarios on Mars (Wordsworth, 2016), surface volcano-ice interaction is a relevant mechanism for habitability (Cousins & Crawford, 2011; Cousins et al., 2018). Glaciovolcanism on Mars may have occurred throughout Mars's history, with the emplacement of lava flows and magma bodies into the planet's cryosphere (Chapman et al., 2000; Cousins & Crawford, 2011; Head and Wilson, 2007). The habitability of hydrothermal systems that result from glaciovolcanic interactions relies on: (i) the phase change of water (from frozen to liquid) enabled by volcanism, (ii) release of gases such as CO₂, H₂S, CH₄, (iii) liberation of essential elements for life from rocks into solution, and (iv) the chemical disequilibrium produced by water-rock interaction and volcanic fluxes, all of which can be exploited by chemoautotrophic organisms (Cousins & Crawford, 2011; Gaidos & Marion, 2003). Glaciers or ground ice deposits paired with volcanic activity could also have provided transient environments for life that persisted into the Amazonian (~3 to 1.1 Ga) (e.g. Scanlon et al., 2014), expanding the temporal range for localised hydrothermal habitats on Mars. Recent direct evidence for such glacier-related hydrothermal systems has been described at Arsia Mons with orbital topographic data (Scanlon et al., 2014, 2015) and Sisyphi Montes with orbital topographic and mineralogical data (Ackiss et al., 2018). Arsia Mons is located south of Tharsis Montes and presents fan-shaped deposits associated with subglacially erupted volcanic edifices (Scanlon et al., 2014, 2015). Some of the morphological evidence indicates wet-based glacial processes, involving the glacier melting at the base due to the heat transfer from the volcano, with ice sliding and subglacial water creating outflow channels (Scanlon et al., 2014, 2015). Sisyphi Montes is a group of volcanic edifices located in a high-latitude region on Mars, the Sisyphi Planum (Tanaka & Scott, 1987). The Sisyphi Montes volcanoes are interpreted to have erupted subglacially, as they present flat top edifices typical of subglacial volcanism (Ackiss et al., 2019). Furthermore, mineralogical assemblages detected (palagonite, smectites, gypsum, sulphates) reveal they were formed in subglacial hydrothermal conditions involving low temperature but high-water/rock ratios (Ackiss et al., 2018). Such hydrothermal systems exemplify habitable alcoves for life on Mars that could have existed throughout much of its history (Michalski et al., 2017; Van Kranendonk et al., 2018; Westall et al., 2015).

While hydrothermal environments are well-recognised as an important habitat for chemolithotrophic microbial life on Earth (Havig et al., 2011) and potentially for early Mars (Pirajno & Van

Summary points

- Environment geochemistry and mineralogy in Mars-analogue hydrothermal systems are controlled by acid supply, redox and secondary mineral solubility, with lithology playing a minor role
- Deep volcanic processes and glacial meltwater input control microbial metabolic function at Mars-analogue hydrothermal environment
- Sulphur- and iron-driven redox metabolisms are dependent on local pH with implications for resulting geochemical biosignatures.

Kranendonk, 2007), only one relict hydrothermal system on Mars has been studied in situ. The Home Plate deposit in Gusev Crater (Columbia Hills) is characterised by high Ti concentrations and deposits of opaline silica (opal Si) in nodular masses (Ming et al., 2008). Together, the high opal Si and Ti concentrations at Home Plate indicate intense basalt leaching, produced by contact with acidic hydrothermal waters (Squyres et al., 2008). The opaline nodule deposits further suggest formation by hydrothermal leaching of basaltic rocks (Skok et al., 2010) or precipitation of silica-sinter deposits (Ruff & Farmer, 2016; Ruff et al., 2011). Such localised and relatively small-scale systems are particularly challenging to investigate from orbit compared with deposits from other potentially habitable environments such as lakes (Hays et al., 2017). However, their small scale is an advantage for surface exploration, as any putative biosignatures are confined to syn-depositional deposits along with the geochemical context for their formation. The localised nature of surface hydrothermal environments can concentrate redox-sensitive mineralogical indicators that can record past surface environmental conditions. Given the possibility for ice-fed hydrothermal systems throughout Mars' history, there is a strong rationale to further our knowledge of their potential as a biological habitat.

We investigated two chemically distinct ice-fed Mars-analogue hydrothermal systems in Iceland to identify the major controls on aqueous geochemistry and the implications for microbial habitability. These systems serve as useful analogues to snow and ice-fed hydrothermal habitats on Mars, such as Sisyphi Montes or Arsia Mons (Ackiss et al., 2018; Scanlon et al., 2014), and also to surface hydrothermal environments fed by meteoric water. A total of six hydrothermal pools in Iceland were used to assess: (i) controls on the dominant aqueous geochemistry in Mars-analogue ice-fed hydrothermal pools; (ii) signatures of aqueous geochemistry recorded by sediment authigenic mineralogy and (iii) implications of geochemistry for the microbial community structure and function. We found that volcanic processes act as the main control of the pool water pH and redox conditions. As a result, volcanism acts as the primary control on microbial community structure and function, whereas the water from the proximal glacier acts as a secondary control by regulating the temperature.

2 | ICELAND ANALOGUE SITES

Iceland's similarities with Mars are wide: availability of extensive mineralogical outcrops, lack of vegetation, little anthropogenic disturbance, perennial sub-zero temperatures and low levels of precipitation (Cousins, 2015). Iceland is a volcanic island, situated above a mantle plume and part of the Mid Atlantic Ridge (Gudmundsson, 2000; Sigvaldason, 1974). The majority of Iceland basalts are tholeiitic, transitioning to alkali (Jakobsson et al., 2008; Sigmarsson & Steinthórsson, 2007). Some Icelandic volcanic basalts are enriched in Fe relative to most terrestrial basalts, resembling the composition of Martian meteorites of mafic to ultramafic composition (shergottites) (Nicholson & Latin, 1992). Due to its high latitude, many of Iceland's volcanoes were once (or still are) covered by glaciers, which lead to subglacial volcanism, drawing parallels with Martian subglacial volcanoes in Tharsis, NE Syrtis, Arsia Mons, Sisyphi Montes and elsewhere (Ackiss et al., 2018; Cassanelli & Head, 2019; Hiesinger & Head, 2004; Scanlon et al., 2014). The Sisyphi Montes glaciovolcanic hydrothermal system (where the mineralogy is dominated by gypsum, smectite-zeolite-iron, palagonite and a polyhydrated sulphate-dominated material) presents similarities to Icelandic glaciovolcanic hydrothermal systems studied by Cousins et al., (2013), who identified gypsum and jarosite, iron oxides, smectites and palagonite. The mineralogy from Arsia Mons has not been studied as a thick mantle of dust inhibits mineralogical spectroscopic measurements (Scanlon et al., 2014). Microbial communities previously investigated in these active Icelandic volcano-ice systems are dominated by microorganisms employing metabolisms such as anaerobic and microaerobic chemolithotrophic Fe reduction, sulphate reduction and sulphide oxidation (Cousins et al., 2018; Gaidos et al., 2009; Marteinson et al., 2013).

2.1 | Kerlingarfjöll

The Kerlingarfjöll volcano ($64^{\circ}38'32.61''\text{N}$, $19^{\circ}17'44.43''\text{W}$) covers an area of $\sim 200 \text{ km}^2$, with the highest peaks (1,000–1,488 m) partially covered by the Hofsjökull glacier (Figures 1a and S1). The volcanic complex formed subglacially between 331 and 65 Ka and has a rhyolitic composition underlain by basalt (Flude et al., 2010; Grönvold, 1972). The reservoir temperatures estimated by gas thermometer calculations from fumaroles indicate Kerlingarfjöll volcanic subsurface temperatures are between 250 and 300°C within the geothermal system (Richter et al., 2010). The northern part of the complex experiences ongoing geothermal activity (Flude et al., 2010; Humlum, 1936). Our area of study is the Vestur-Hveradalir valley area. Here, meltwater from the glacier interacts with fumaroles downstream, forming a series of pools (Humlum, 1936; Figure 1b–d).

2.2 | Kverkfjöll

The Kverkfjöll volcano ($64^{\circ}41'22.28''\text{N}$, $16^{\circ}40'43.01''\text{W}$) underlies the northern margin of the Vatnajökull glacier (Figures 1a and S1). Kverkfjöll eruptions date back to $\sim 7.6 \text{ Ka}$ (Óladóttir et al., 2011a). It rises 1,000 m above the local area and has two calderas with an associated NW-extending fissure swarm (Björnsson & Pálsson, 2008). The volcanic complex hosts a high-temperature geothermal area at the glacier margin, covering 25 km^2 , with a surface manifestation of pools, mudpots and fumaroles (Figure 1f–h). Most of the exposed geothermal areas lie within the northern caldera (Ármannsson, 2016; Cousins et al., 2013, 2018; Ólafsson et al., 2000). Gas thermometer calculations indicate the Kverkfjöll volcanic subsurface temperature is $\sim 300^{\circ}\text{C}$ within the geothermal system (Ólafsson et al., 2000). Eruptive materials are tholeiitic basalts (Jakobsson et al., 2008)

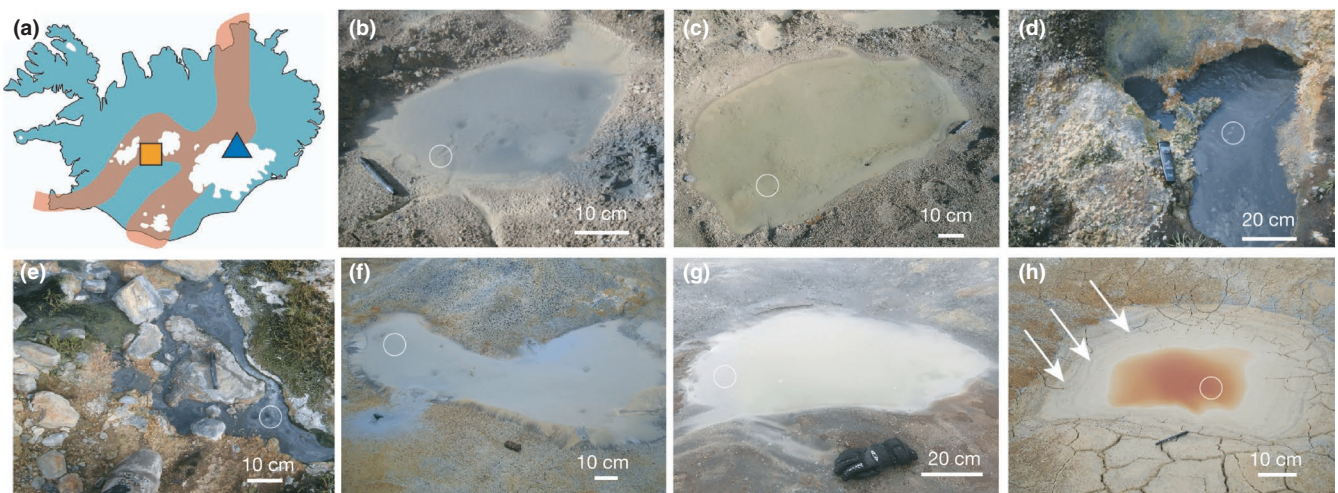


FIGURE 1 (a) Map of Iceland with Volcanic Rifting Zone in orange, Kerlingarfjöll (square), and Kverkfjöll (triangle). Kerlingarfjöll pools with a circle where the sample was taken: (b) KR-P1, pen for scale, (c) KR-P2, pen for scale, (d) KR-P3, pH meter for scale, (e) KR-Bio, pen for scale. Kverkfjöll pools: (f) KV-P4, camera for scale, (g) KV-P5, glove for scale, (h) KV-P6, pen for scale, arrows show evaporation marks

including hyaloclastite, pillow lava and fine-grained tuff sequences (Óladóttir et al., 2011b). The study area, Hveratagl, is situated on the northern caldera ridge. Here, as with Kerlingarfjöll, the geothermal features investigated comprise snow/ice-fed meltwater pools interacting with the fumarolic ground (Figure 2). Previous studies in Kverkfjöll identified pools with a pH of 3–4, temperatures ranging from 10 to 20°C (Cousins et al., 2013) and alteration phases including zeolites (heulandite), sulphates (gypsum, jarosite, alunogen), crystalline Fe-oxides (goethite, hematite), smectite (montmorillonite, saponite) and ferric oxides. Similar alteration phases have also been detected at Sisyphi Montes on Mars by orbit, including gypsum, polyhydrated sulphates, smectites, zeolites and iron oxides (Ackiss et al., 2018).

3 | METHODS

3.1 | Field sampling

Water and sediment samples were collected in August 2017 from pools with either visible or absent fumarole steam input (e.g. observed active gas bubbles), capturing a range of colour variations indicative of compositional differences. Pool sizes were between 30 cm and 1.5 m in diameter. In most pools, the observed bubbles in the water resulted from volcanic gas input rather than from boiling, as the temperatures of the pools were between 20 and 60°C. Three pools were sampled within the Kerlingarfjöll Hvestur-Hveradallir valley: (i) KR-P1 (water with gas input; Figure 1b), and (ii) KR-P2 (no visible gas input; Figure 1c), both about 2 m downslope from the glacier; and (iii) KR-P3 (gas input and black sediments; Figure 1d), which was located on an contiguous slope, only a 50 m from KR-P2. Lastly, a meltwater stream was sampled at the adjacent valley, 500 m SE (KR-Bio; Figure 1e). At Kverkfjöll three pools were sampled: (i) KV-P4 (with visible gas input; Figure 1f); (ii) KV-P5 (with no gas input; Figure 1g); and (iii) KV-P6 (which had a strong red colouration and no visible gas input; Figure 1h). Snowpack samples were taken close to the pools at both Kerlingarfjöll (KR-ice) and Kverkfjöll (KV-ice) for SO_4^{2-} and Cl^- measurements. Sediment sample locations within the pools are shown in Figure 1; sediments were taken from up to 2–5 cm depth at the sediment–water interface to capture the authigenic alteration environment, with approximately 50 ml of wet sediment collected.

Temperature, pH and dissolved oxygen (DO) were measured in situ using a Mettler Toledo meter (± 0.02 pH error, $\pm 1\%$ DO), calibrated in the field. Thermal imaging was achieved using a Testo 882 thermal camera. Waters for ionic analyses from pools were filtered through 0.2 μm Surfactant-free Cellulose Acetate (SFCA) filters and subsequently stored in polypropylene 15 ml tubes at $\sim 4^\circ\text{C}$. Duplicates were acidified in the field with 1% HNO_3 and preserved for analysis of (i) dissolved major cations (Ca, Fe, Si, Al, Mg, Na, K, Pb, Zn, Cr, Mn, P) and (ii) H-O isotope and Cl^- analyses. Water samples for dissolved SO_4^{2-} and H_2S were collected by filtering the water through 0.2 μm SFCA filters. The H_2S was fixed immediately as ZnS

with 0.5% ZnCl_2 , in 15ml tubes in the field. Samples for DNA extraction were collected in sterile 50 ml tubes, transported on ice and frozen at -20°C immediately upon return to the laboratory until DNA extraction.

3.2 | Water chemistry and isotope composition

Cations were measured using a Prodigy7 (Teledyne-Leeman) ICP-OES. Mean values were taken from three replicate analysis per sample, and a standard was measured every 5th measurement to assess the drift of the ICP-OES. The accuracy of the results is reported with the Minimum Detection Limit (MDL) value (between 0.01 and 0.04 ppm, Table 1), which show the precision of the measurement for each element.

Anions were measured in triplicate using ion chromatography with a Metrohm 930 Compact IC Flex. Standard deviations of measurements were $\leq 0.1\%$ for all anions. Sulphide concentrations were measured photometrically using the methylene blue method ($\pm 2\%$ precision with 95% confidence; Cline, 1969) with a Thermo Scientific GENESYS 10S Series Uv-Vis Spectrophotometer. Hydrogen and oxygen isotope values of water oxygen ($^{18}\text{O}/^{16}\text{O}$; $\delta^{18}\text{O}$) and hydrogen ($^2\text{H}/^1\text{H}$; δD) were measured by cavity ringdown spectroscopy using an L2140-i Picarro interfaced with an A0211 high-precision vaporiser. Isotopic results are given as δ -values (‰) for V-SMOW (Vienna-Standard Mean Ocean Water), and analytical precisions were better than 0.05 ‰ for $\delta^{18}\text{O}$ and 0.4 ‰ for δD . All analyses were conducted at the University of St Andrews, UK, except for cation analyses, which were performed at the Open University, UK.

Eh-pH diagrams were constructed in the ACT2 module of the Geochemist's Workbench (GWB14 Professional) software with the 'thermo' database (Bethke, 2011). The Eh values were calculated using the GSS module.

3.3 | Mineralogy and major element composition

Sediments were freeze-dried (~ 5 g), homogenised and ground to <150 μm to be analysed for major element composition by Energy-Dispersive X-Ray Fluorescence (XRF) using a Spectro XEPOS HE at the University of St Andrews. XRF analysis was carried out on glass discs prepared by fusing 0.5 g of sample with 5 g of flux (50:50 mix lithium tetraborate and lithium metaborate). For X-Ray Diffraction (XRD) analysis of crystalline sediment components, samples were further hand ground to <5 μm in a mortar and pestle. These powders were mixed with a NIST SRM ZnO 674 b internal standard (10% ZnO by weight), loaded into a 0.7 mm diameter borosilicate glass capillary and mounted onto the powder diffraction beamline at the Australian Synchrotron (Wallwork et al., 2007). The wavelength was determined using NIST SRM LaB6 660 b to be 0.7769787 (5) Å. Data were collected using the Mythen II microstrip detector (Schmitt et al., 2003) from 1.5 to 76° in 2 theta. To cover the gaps between detector modules, two data sets, each of 5 min in duration,

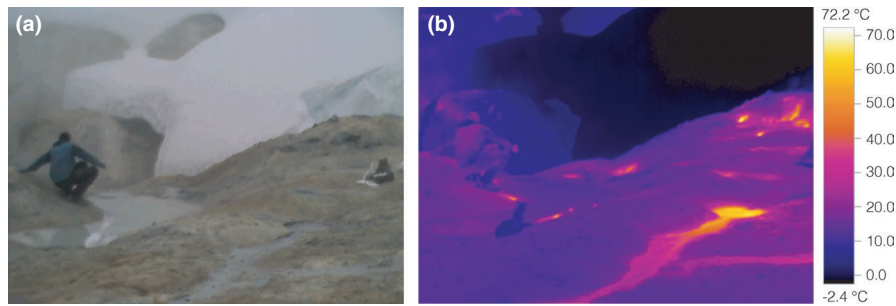


FIGURE 2 Thermal image from Hveratagl, Kverkfjöll, with geologist for scale in front of pool KV-P4. This shows the spatial association between fumarole clusters (maximum temperature 72.2°C) and compacted snow (minimum temperature -2.4°C), forming the thermal end-members within this environment. The meltwater pool of the pictures (KV-P4) displays an intermediate temperature (20.3°C)

were collected with the detector set 0.5° apart and these were then merged to give a single data set. Merging was performed using the in-house software PDViPER. The capillary was rotated at ~1 Hz during data collection to aid powder averaging. Mineral phases present were determined using a Panalytical high score with the ICDD PDF4+ database. Semi-quantitative phase analysis was carried out in Topas version 6 (Bruker AXS), using the internal standard method to determine relative amounts of the crystalline material.

3.4 | DNA extraction

Total genomic DNA was extracted from sediment samples using the Qiagen DNAeasy PowerMax Soil Kit (Qiagen laboratories, Germany) following the manufacturer's instructions, modified with the addition of 1 M phosphate buffer (adapted from Direito et al., 2012) to minimise clay adsorption of nucleic acids. To mitigate against extraction bias, duplicate extractions comprising a 'soft' and 'hard' method were conducted. For each, 1 g of sample was used for the extraction, with 4 ml of 1 M phosphate buffer added to the bead-beating tubes, and then, the mix was gently inverted twice and incubated for 30 min at 60°C before continuing with the DNA isolation protocol. For the soft extraction, the bead-beating step was replaced with a further 30-min incubation at 60°C temperature. After extraction, the DNA was concentrated from 5 ml to a final volume of 1 ml using 5 M NaCl and 100% cold ethanol, and hard and soft extractions were pooled before sequencing.

PCR amplification was used to screen for positive 16S rRNA gene products for bacteria and archaea. Each 50 µl PCR reaction contained 25 µl of REDTaq Ready Mix with MgCl₂ (Sigma-Aldrich), 0.5 µl forward primer (either 21F- TTC CGG TTG ATC CYG CCG G for archaea or 27F-AGA GTT TGA TYM TGG CTC AG for bacteria), 0.5 µl of reverse primer (UN1492R-GGT TAC CTT GTT ACG ACT T), 1 µl template DNA and 23 µl of nuclease-free water. PCR conditions were as follows: denaturing at 94°C for 3 min, annealing at 53°C for 40 s and elongation at 72°C for 90 s, with a final elongation step of 72°C extended for 90 s. The PCR cycle was repeated 30 times and PCR products verified with gel electrophoresis (Primers and PCR conditions from DeLong (1992)).

PCR screening was also conducted for the gene that encodes the APSr enzyme (adenosine-5'-phosphosulphate reductase) (Friedrich, 2002), used here as a proxy for sulphur metabolism potential of the microbial community. PCR master mix was prepared as above using forward primer APSF-TGGCAGATMATGATYMACGG and reverse primer APSR- GGGCCGTAACCGTCCTTGAA (Friedrich, 2002). The thermal cycle for PCR was as follows: denaturing stage at 94°C for 2 min, annealing at 60°C for 1 min and elongation at 72°C for 3 min, with a final elongation of 72°C extended for 10 min (Friedrich, 2002). The PCR cycle was repeated 30 times and products visualised using gel electrophoresis.

3.5 | DNA sequencing and analysis

Circular Consensus Sequencing was performed by MR DNA (Shallowater, TX, USA) on the PacBio Sequel using bacteria (27F-AGAGTTTGATCCTGGCTCAG and 519R-GTNTTACNGCGGCKGC TG) and archaea (21F- TCCGGTTGATCCYGCCGG and 505R- CCR TGC TTS GGR CCV GCC TGV CCG AA) specific primers. A depth of 5,000 reads per sample was achieved for each 16S rRNA assay with an average post-processing read length of 1,400 bp. Sequence data were processed using the MR DNA analysis pipeline to remove barcodes, orientate sequences 5' to 3', and to remove sequences <150 bp and sequences with ambiguous base calls. Sequences were denoised, OTUs generated and chimeras removed. Operational taxonomic units (OTUs) were defined by clustering at 97% similarity. Final OTUs were taxonomically classified using BLASTn against a curated database derived from RDP II (<http://rdp.cme.msu.edu>) and NCBI (www.ncbi.nlm.nih.gov). Downstream bioinformatics analysis of OTU sequences was performed using Mothur (v. 1.42.3; Schloss et al., 2009), following an adapted protocol from Wagner et al. (2016). Briefly, sequences <1,400 bp and >1,500 bp were removed using screen.seqs command and the remaining sequences aligned with the Silva reference database (v. 132, Quast et al., 2012). Aligned sequences were further screened to remove alignments outside of expected positions (start = 1,046, end = 43,116) and filtered using filter.seqs to remove empty columns. Filtered sequences were used to generate a phylip-formatted distance matrix using a cutoff of 0.03

TABLE 1 Geochemical parameters of pools. BD = below detection. DO = Dissolved Oxygen. All values reported as ppm unless otherwise stated. MDL = Minimum Detection Limit for each element in ppm

Site	Kerlingarfjöll		Kerlingarfjöll		Kerlingarfjöll		Kerlingarfjöll		Kerlingarfjöll		Kerlingarfjöll	
	KR-P1	KR-P2	KR-P3	KR-Bio	KV-P4	KV-P5	KV-P6	MDL	KR-ice	KV-ice		
Temperature (°C)	22.30	21.60	>60	52.0	20.30	23.60	16.80	-	-	-		
pH	6.00	6.50	5.50	7.35	2.70	1.94	1.76	-	-	-		
DO	0.06	0.93	0.80	2.47	0.26	2.00	1.57	-	-	-		
Si	13.25	4.13	27.52	20.87	12.55	54.38	78.27	0.01	-	-		
Ca	195.73	162.24	60.46	39.27	0.21	79.60	54.38	0.01	-	-		
Na	34.93	13.73	39.49	36.00	BD	4.97	7.00	0.11	-	-		
K	6.48	1.84	6.62	3.68	0.22	0.35	0.27	0.01	-	-		
Fe _{total}	0.55	BD	BD	BD	7.10	2050.91	4,156.32	0.03	-	-		
Mg	113.79	38.73	13.51	17.41	BD	72.05	92.89	0.02	-	-		
Mn	4.43	1.19	0.58	0.30	0.04	5.53	7.37	0.01	-	-		
Al	BD	BD	BD	BD	1.33	386.00	910.65	0.04	-	-		
Pb	BD	BD	BD	BD	BD	BD	BD	0.01	-	-		
Cr	BD	BD	BD	BD	BD	2.88	5.95	0.02	-	-		
P	BD	BD	BD	BD	BD	1.01	3.08	0.02	-	-		
Zn	BD	BD	BD	BD	BD	2.170	2.488	0.01	-	-		
Cl ⁻	0.85	0.81	2.01	2.64	0.21	3.00	2.10	2.32	3.97	-		
SO ₄ ²⁻	937.75	542.47	333.87	108.28	61.71	13,888.82	21,001.12	13.11	6.16	-		
Total ions	1,310.13	767.69	486.91	231.34	85.76	16,608.50	26,438.99	-	-	-		
H ₂ S	1.54	0.05	2.57	1.25	BD	-	BD	-	-	-		
δ ¹⁸ O (‰)	0.55	-5.39	-3.54	-7.07	-10.63	-4.65	-0.95	-9.16	-10.50	-		
error std	0.06	0.03	0.02	0.03	0.01	0.07	0.08	0.04	0.03	-		
δD(‰)	-55.29	-70.00	-79.92	-86.11	-87.15	-68.36	-45.35	-60.44	-78.66	-		
Error std	0.16	0.29	0.09	0.19	0.13	0.19	0.27	0.16	0.15	-		

and a phylogenetic tree created using command `clearcut`. The similarity between Kverkfjöll- and Kerlingarfjöll-hosted pools for both bacteria and archaea was visualised using `tree.shared`. All trees were visualised using the Interactive Tree of Life (Letunic & Bork, 2019).

Lastly, FAPROTAX (Functional Annotation of Prokaryotic Taxa, Louca et al., 2016) was used to assign predicted microbial metabolic functions, converting taxonomic microbial community profiles into functional profiles, using default parameters. The files used to construct the plots were sequence counts, which are the actual number of sequences counted for a designated taxonomic classification.

Sequenced data are available at the NCBI database (<https://www.ncbi.nlm.nih.gov/biosample>), under submission number SUB7731879. The BioSample accession numbers are SAMN15482945 to SAMN15482949 for archaeal data and SAMN15482950 to SAMN15482956 for bacteria.

4 | RESULTS

4.1 | Water geochemistry

Rhyolite-hosted (Kerlingarfjöll) and basalt-hosted (Kverkfjöll) pools show clear physicochemical distinctions (Figure 3, Table 1). In particular, pH delineates these two sites: Kerlingarfjöll is acidic to neutral (pH from 5.5 to 7.3), whereas Kverkfjöll is acidic (pH from 1.7 to 2.7). The aqueous chemistry at both sites is dominated by SO_4^{2-} (up to 937.75 ppm at Kerlingarfjöll, and up to 21,000.01 ppm at Kverkfjöll),

but differences in water composition can be seen in the other dominant ions (Figure 3e). Dissolved oxygen concentrations are variable across all sites: microoxic conditions characterise Kerlingarfjöll pools (0.06 ppm at KR-P1, 0.93 ppm at KR-P2, 0.80 ppm at KR-P3) and Kverkfjöll KV-P4 (0.26 ppm), while oxic conditions are found in KR-Bio (average of dissolved oxygen is 2.47 ppm), and at Kverkfjöll in KV-P5 and KV-P6 (2.00 ppm and 1.57 ppm, respectively). Pool temperatures at both sites are between 16 and 23°C, apart from Kerlingarfjöll KR-P3 and KR-Bio, at 60°C and 52°C, respectively.

Kerlingarfjöll pools have high concentrations of total dissolved Ca, Mg, K, Na, H_2S (0.05–2.5 ppm) and undetectable total Al and Fe (the only pool with detectable Fe was KR-P1, with 0.55 ppm). Conversely, Kverkfjöll acidic waters are dominated by high concentrations of total Al and total Fe (7.15–2050.91 ppm), with no detectable H_2S . Chloride concentrations at both sites are low, ranging from 0.81 to 2.64 ppm for Kerlingarfjöll pools, similar to the nearby snowpack sample (KR-ice, 2.32 ppm). Chloride concentrations for the Kverkfjöll pools (0.21–2.99 ppm) are lower than that of the snowpack sample (KV-ice, 3.97 ppm; Figure 3b). Only Kverkfjöll has ppm levels of total Mn, P, Zn and Cr, which were not detected at Kerlingarfjöll.

Both Kerlingarfjöll and Kverkfjöll pool waters show $\delta^{18}\text{O}$ and δD values (Figure 3d) deviating from the Icelandic Water Meteoric Line (IWML; MacDonald et al., 2016). The waters with the highest $\delta^{18}\text{O}$ and δD values are KR-P1 and KV-P6 (temperatures of 22 and 16°C, respectively), for which pools have no visibly apparent active water inlets or outlets at the time of sampling. At Kverkfjöll, the $\delta^{18}\text{O}$ and δD values are higher than those reported in a previous study that

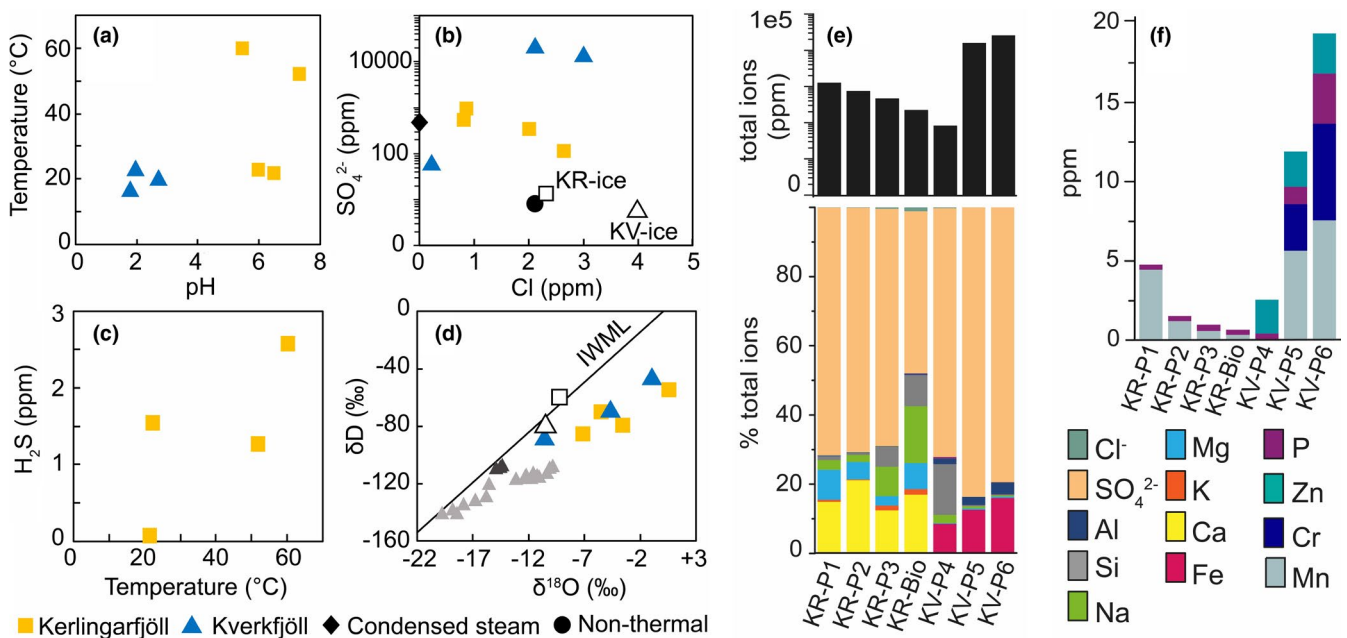


FIGURE 3 Water chemistry for Kerlingarfjöll and Kverkfjöll pools. (a) Temperature vs pH; (b) SO_4^{2-} vs. Cl^- ; condensed steam and non-thermal shown for comparison (values from Stefánsson et al., 2016); (c) H_2S concentrations vs Temperature, Kverkfjöll H_2S concentrations are below detection; (d) δD vs $\delta^{18}\text{O}$. Icelandic Water Meteoric Line (IWML) data from MacDonald et al. (2016). Grey triangles show previous data from Kverkfjöll steam (light grey) and water (black) (Ólafsson et al., 2000). (e) Total ion concentration in solution (log scale) and relative percentage of dissolved anions and cations. (f) Expanded plot for ions <2% abundance (Mn, Cr, P, Zn) in ppm

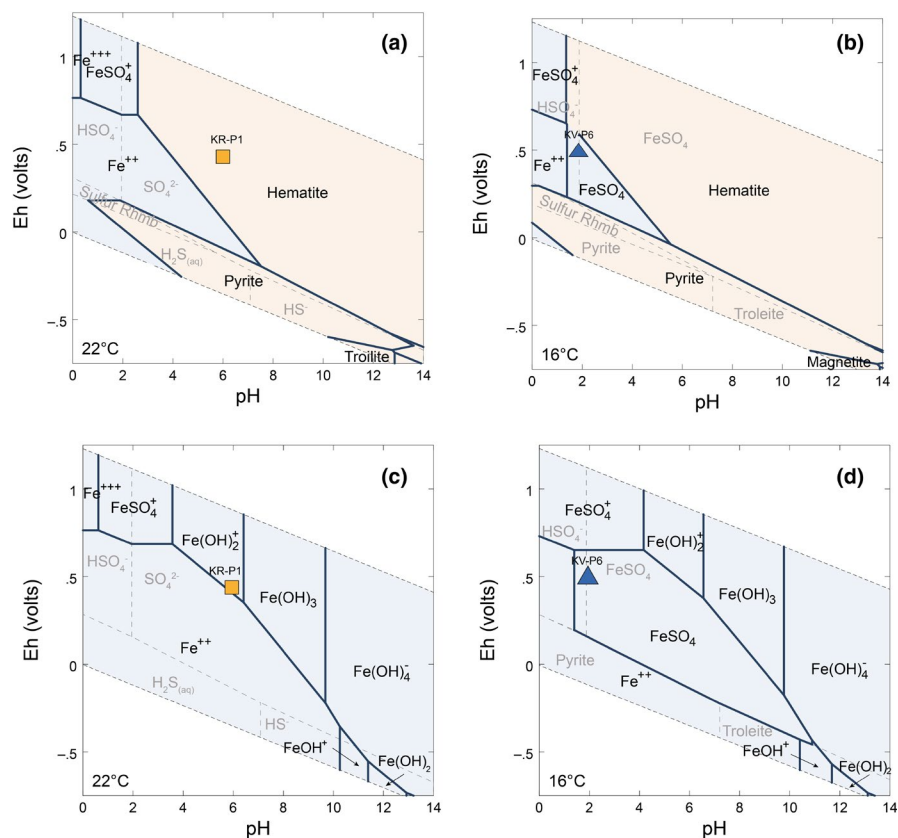


FIGURE 4 Eh-pH diagrams for iron species, with sulfur stability fields marked with dashed lines for two representative pools from Kerlingarfjöll and Kverkfjöll. Diagrams for mineral stability fields for (a) KR-P2 and (b) KV-P6. Diagrams for water species stable at (c) KR-P2 and (d) KV-P6

TABLE 2 Table below shows XRD results with percentages (+/- 5%) of each phase present on the sediment sample. n/a = not applicable

Site	Sample ID	Quartz	Pyrite	Calcite	Anatase	Kaolinite	Montmorillonite
Kerlingarfjöll	KR-P1	65	5	15	n/a	10	5
Kerlingarfjöll	KR-P2	60	5	10	5	15	5
Kerlingarfjöll	KR-P3	30	30	n/a	10	25	5
Kerlingarfjöll	KR-Bio	55	25	5	5	5	5
Kverkfjöll	KV-P4	n/a	20	n/a	15	60	5
Kverkfjöll	KV-P5	n/a	15	n/a	10	70	5
Kverkfjöll	KV-P6	n/a	15	n/a	15	65	5

measured stable isotopes in steam from fumaroles and water from the same area (Ólafsson et al., 2000). This same study measured the gas from the fumaroles in Kverkfjöll showing a resulting composition of 80%–97% of CO_2 , 1%–12% of H_2S and 0.2% of CH_4 .

The calculated Eh-pH diagrams for Fe and S speciation are shown in Figure 4 with a representative sample from each site (KR-P1 from Kerlingarfjöll and KV-P6 from Kverkfjöll; the diagrams from all pools can be found in Figures S2–S5). The main stable aqueous species of S in Kerlingarfjöll pools is SO_4^{2-} (Figure S2), whereas in Kverkfjöll it is the aqueous ion pair FeSO_4^0 (Figure S3). The most abundant stable aqueous Fe species in Kerlingarfjöll are $\text{Fe}(\text{OH})_2^-$ and $\text{Fe}(\text{OH})_3^0$ and in one case $\text{Fe}(\text{SO}_4)_2^-$. In all of these species (Figures 4 and S4), Fe is in the +3 redox state. In contrast, Kverkfjöll is dominated by Fe^{2+} -species in the form of either free Fe^{2+} (KV-P4) or FeSO_4^0 (KV-P5 and KV-P6) (Figures 4 and S5). When iron minerals are included in the plots (Figure 4a,b), all Kerlingarfjöll fluids are in equilibrium with hematite, a Fe^{3+} mineral. At Kerlingarfjöll, three out of four samples

plot outside any mineral stability field, indicating that these fluids are not in direct equilibrium with a mineral phase. The sample KV-P4 is in equilibrium with hematite.

4.2 | Sediment mineralogy and geochemistry

Bulk mineralogy derived from XRD analysis is presented in Table 2 and Figure 5. XRD patterns for Kerlingarfjöll sediments have sharper peaks than those measured from Kverkfjöll sediments, with the latter exhibiting broad amorphous peaks, indicating more X-ray-amorphous phases are present (Figure 5, Table 2). Crystalline phases detected by XRD in Kerlingarfjöll sediments include quartz, calcite, kaolinite, montmorillonite and anatase, while pyrite dominates the sediment from KR-P3 and KR-Bio. Kverkfjöll sediment XRD patterns indicate kaolinite, pyrite, anatase and montmorillonite. The relative abundance of kaolinite distinguishes the two field areas, whereby

kaolinite in Kerlingarfjöll pools accounts for ~10% to 25% crystalline phases compared to ~60% to 70% in Kverkfjöll pool sediments.

XRF bulk major elemental composition data show Kerlingarfjöll and Kverkfjöll sediments are all depleted in SiO_2 , Na_2O and K_2O ,

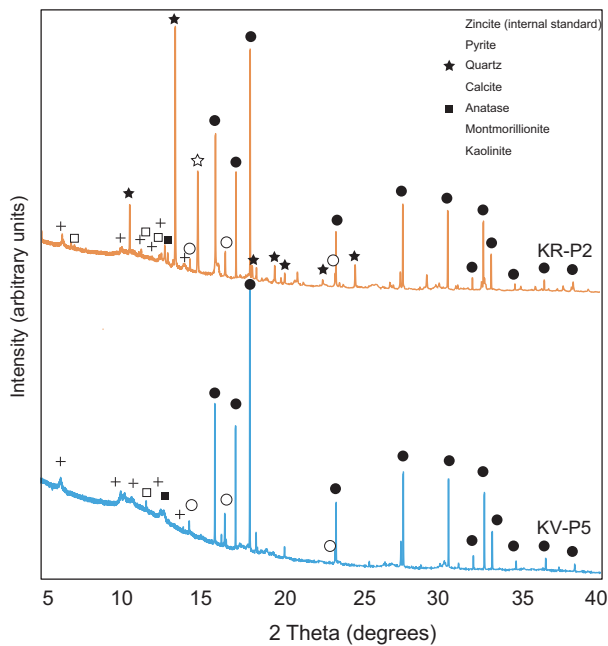


FIGURE 5 Representative XRD patterns from Kerlingarfjöll (KR-P2) and Kverkfjöll (KV-P5) bulk sediment. Major peaks for mineral phases marked with symbols

and Kverkfjöll sediments enriched in Al_2O_3 and TiO_2 (Figure 6 and Table 3), in relation with their host lithologies. Kerlingarfjöll sediments are also enriched in MgO and CaO , the latter consistent with the XRD detection of calcite. Open-system Chemical Index of Alteration (CIA = $\text{Al}_2\text{O}_3/(\text{Al}_2\text{O}_3 + \text{CaO} + \text{K}_2\text{O} + \text{Na}_2\text{O})$; Nesbitt & Young, 1982) values at Kerlingarfjöll range from 52% to 78%, and 96% to 98% at Kverkfjöll. The ternary AFK plot (Figure 6f) supports this high degree of enrichment in Al relative to major cations, with Kverkfjöll sediments progressing further along the path of argillic weathering, compared with Kerlingarfjöll, which instead is slightly enriched in FeO and MgO , following a more typical terrestrial weathering profile (Hurowitz et al., 2006; Nesbitt & Young, 1984).

4.3 | Archaeal communities

Archaeal communities were similar across all pools at the phylum level, dominated by the Crenarchaeota and Euryarchaeota (Figure 7a). At the genus level, the archaeal communities in the Kerlingarfjöll pools and KR-Bio are dominated by sequences that affiliate with ~ (38%–65% relative abundance Figure 7b, Tables S1 and S2). The Kerlingarfjöll pool archaeal communities also composed of a variety of methanogenic genera (*Methanobrevibacter*, *Methanomassiliicoccus*, *Methanosaeta*, *Methanothermobacter*, *Methanococcus*, *Methanocaldococcus*, *Methanocella* and *Methanotorris*). The KR-Bio population conversely has few methanogens (*Methanotorris*, 1.5%). The ammonia oxidising archaeon *Candidatus Nitrosocaldus* is the only genus found across both Kerlingarfjöll and Kverkfjöll (Figure 8c), and at KV-P5 makes up ~50%

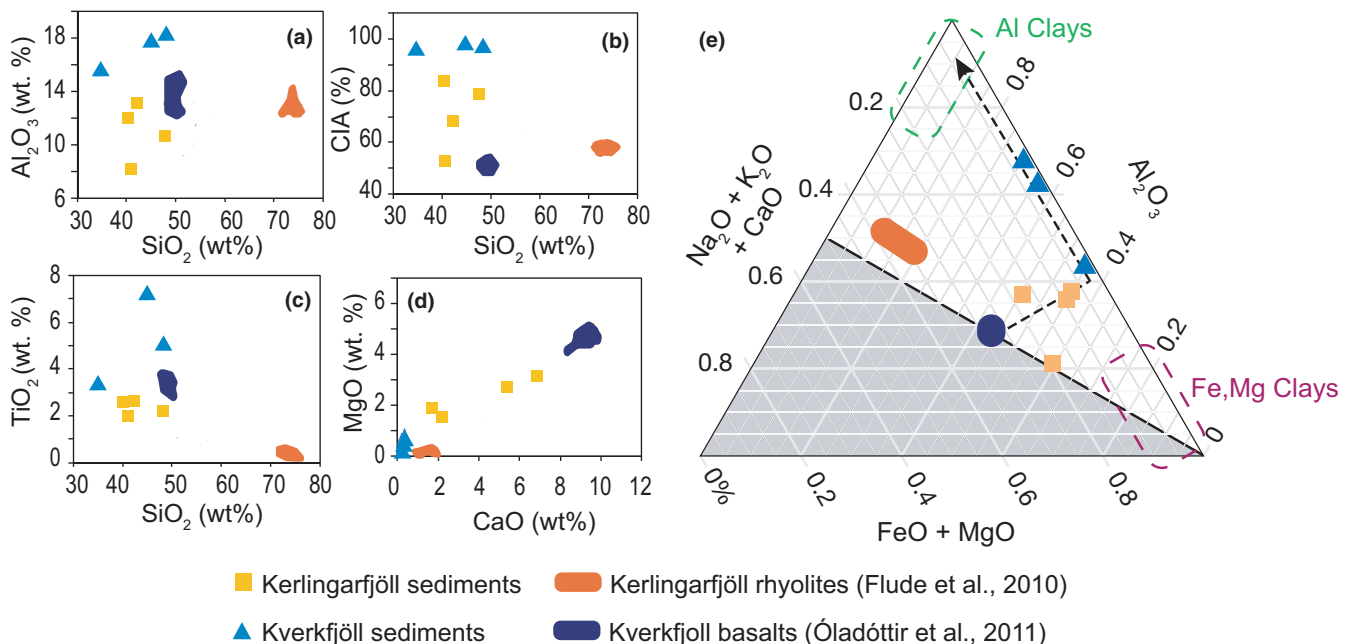


FIGURE 6 Elemental composition data for Kverkfjöll and Kerlingarfjöll pool sediments. (a) Al_2O_3 vs SiO_2 (wt. %). (b) CIA weathering index vs SiO_2 (wt. %). (c) TiO_2 vs SiO_2 (wt. %). (d) MgO vs CaO (wt. %). (e) Ternary AFK diagram, adapted from Hurowitz et al. (2006) and Ehlmann et al. (2011). Dashed black arrow indicates the main basalt alteration pathway. Data for Kerlingarfjöll rhyolites and Kverkfjöll basalts from Flude et al. (2010) and Óladóttir et al. (2011b) respectively

TABLE 3 Table with elemental chemistry data results for both sites

Site	Kerlingarfjöll	Kerlingarfjöll	Kerlingarfjöll	Kerlingarfjöll	Kerlingarfjöll	Kerlingarfjöll	Kerlingarfjöll	Kerlingarfjöll	Kerlingarfjöll	Kerlingarfjöll	Kerlingarfjöll
Sample ID/ Major elements (wt%)	KR-P1	KR-P2	KR-P3	KR-Bio	KV-P4	KV-P5	KV-P6	absolute deviation (avg)	relative deviation (%)	Average values for rhyolitic host rock (Flude et al., 2010)	Average values for basaltic host rock (Óladóttir et al., 2011)
SiO ₂	42.36	41.0	40.38	48.03	44.9	34.65	48.24	0.05	0.1	74.41	49.62
TiO ₂	2.57	1.82	2.52	2.23	7.24	3.36	5.04	0.00	0.0	0.22	3.25
Al ₂ O ₃	13.03	8.08	11.94	10.56	17.83	15.55	18.36	-0.20	-1.6	12.78	13.41
FeO	14.51	18.86	14.52	13.57	9.99	19.98	7.43	0.01	0.4	2.90	14.33
MnO	0.23	0.31	0.14	0.17	0.02	0.04	0.03	0.00	-1.2	0.08	0.23
MgO	2.68	3.17	1.93	1.53	0.33	0.91	0.72	-0.04	-2.4	0.08	4.82
CaO	5.38	6.87	1.7	2.17	0.18	0.36	0.22	-0.03	-0.6	1.12	9.18
Na ₂ O	0.43	<0.13	0.18	0.26	<0.11	<0.12	0.11	0.11	6.7	4.83	2.82
K ₂ O	0.41	0.31	0.49	0.47	0.06	0.18	0.19	0.02	0.8	3.54	0.61
P ₂ O ₅	0.34	0.27	0.29	0.34	0.38	0.43	0.42	0.00	-1.8		
SO ₃ *	1.92	3.22	0.81	0.90	0.04	0.14	0.17				
CIA (%)**	67.6	52.9	83.4	78.4	98.6	96.6	97.2				
Na ₂ O+K ₂ O	0.84	0.31	0.67	0.73	0.06	0.18	0.30				
LOI (%)	15.95	15.73	24.91	19.58	18.83	24.24	18.92				
SUM	97.89	96.53	99	98.92	99.74	99.7	99.67				

*Sulphates measured (total S in the sample, part of LOI) semiquantitative measurement. This is not volatilised sulphides.; **CIA = $(Al_2O_3/(Al_2O_3 + CaO + K_2O + Na_2O)) \times 100$.

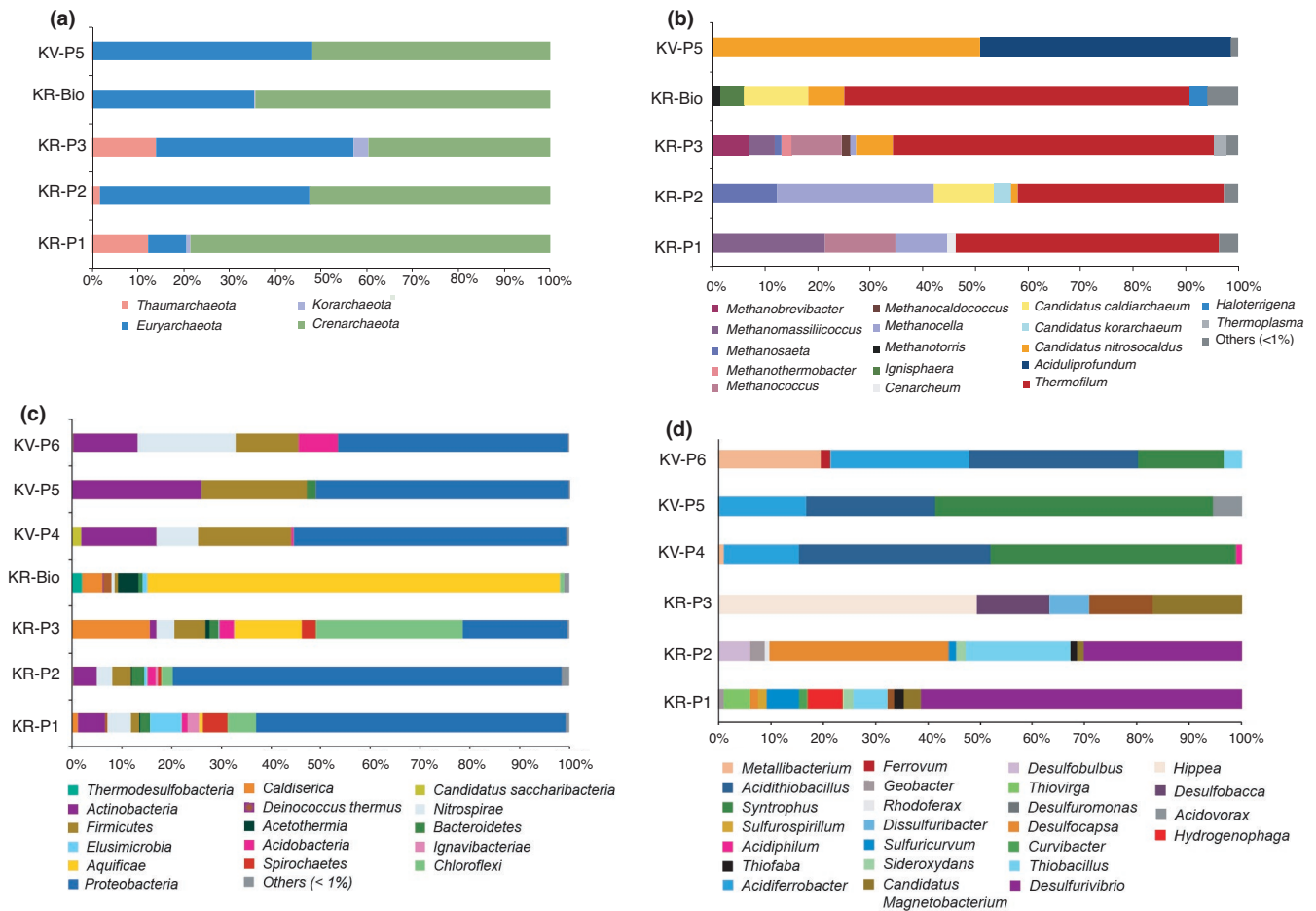


FIGURE 7 Phylogenetic affiliation of OTUs for Archaea at (a) phylum level, (b) genus level, and for Bacteria at (c) phylum level and (d) Proteobacteria in genus level - KR-Bio is not featured as Proteobacteria make up less than 1% of the profile

of the community profile (Figure 7b). Archaeal genera found at KV-P5, however, are still distinct from those at Kerlingarfjöll (Figure 8e), despite their similarity at the phylum level (Figure 7a).

4.4 | Bacterial communities

Proteobacteria are the most abundant phylum across Kerlingarfjöll pools KR-P1 and KR-P2 and all three Kverkfjöll pools (46%–77%, Figure 7c, Tables S3–S5). The remaining community profiles between KR-P1 and KR-P2 are similar (Figure 7c) with varying abundances of Actinobacteria (1%–5%), Nitrospirae (3%–5%), Firmicutes (2%–6%), Acidobacteria (1%–3%), Spirochaetes (1%–3%) and Chloroflexi (2%–29%). At Kverkfjöll pools, the remaining phylum profiles have likewise similar taxonomic affiliations, dominated by Actinobacteria (13%–26%), Nitrospirae (8%–20%) and Firmicutes (12%–21%). Within the Proteobacteria, *Desulfurivibrio* represents 35% of the profile at genus level in KR-P1 and 21% in KR-P2 (Figure 7d). KR-P2 Proteobacteria also includes *Desulfocapsa* (24%) and *Thiobacillus* (14%), while Kverkfjöll pools are dominated by *Syntrophus* (7%–25%), *Acidithiobacillus* (9%–24%) and *Acidiferrobacter* (6%–12%) (Figure 7d). Kerlingarfjöll sites KR-P3 and KR-Bio are not dominated by Proteobacteria. At KR-Bio,

Proteobacteria make up <1% of the bacterial community, and only 22% for KR-P3 (Figure 7c). Instead, KR-Bio is dominated by Aquificae (82%), of which OTUs are dominantly *Sulfurihydrogenibium* (75%).

Phylogenetic trees for Bacteria and Proteobacteria across all sites are shown in Figure 8. Despite being a relatively small component of most pools in terms of sequence reads, Chloroflexi members exhibit a high diversity at the genus level. Proteobacteria likewise exhibit many distinct OTUs, with Kerlingarfjöll pool communities comprising an array of α -, β -, γ - and δ -Proteobacteria, while Kverkfjöll pool proteobacterial diversity is largely limited to the γ -Proteobacteria. The dendrogram (Figure 8d) groups Kerlingarfjöll pools into two clusters: KR-P1 and KR-P2, and KR-P3 and KR-Bio. Kverkfjöll pool OTUs are distinctive from Kerlingarfjöll pool OTUs, with KV-P4 and KV-P6 sharing more bacterial clades than with KV-P5.

4.5 | Inferred metabolisms

Microbial metabolism inferred using FAPROTAX (Louca et al., 2016) is provided in Figures 9 and 10. The dominant archaeal metabolic pathways (Figure 9 and Table S6) identified within Kerlingarfjöll pools are sulphur respiration (S^0), methanogenesis and ammonia

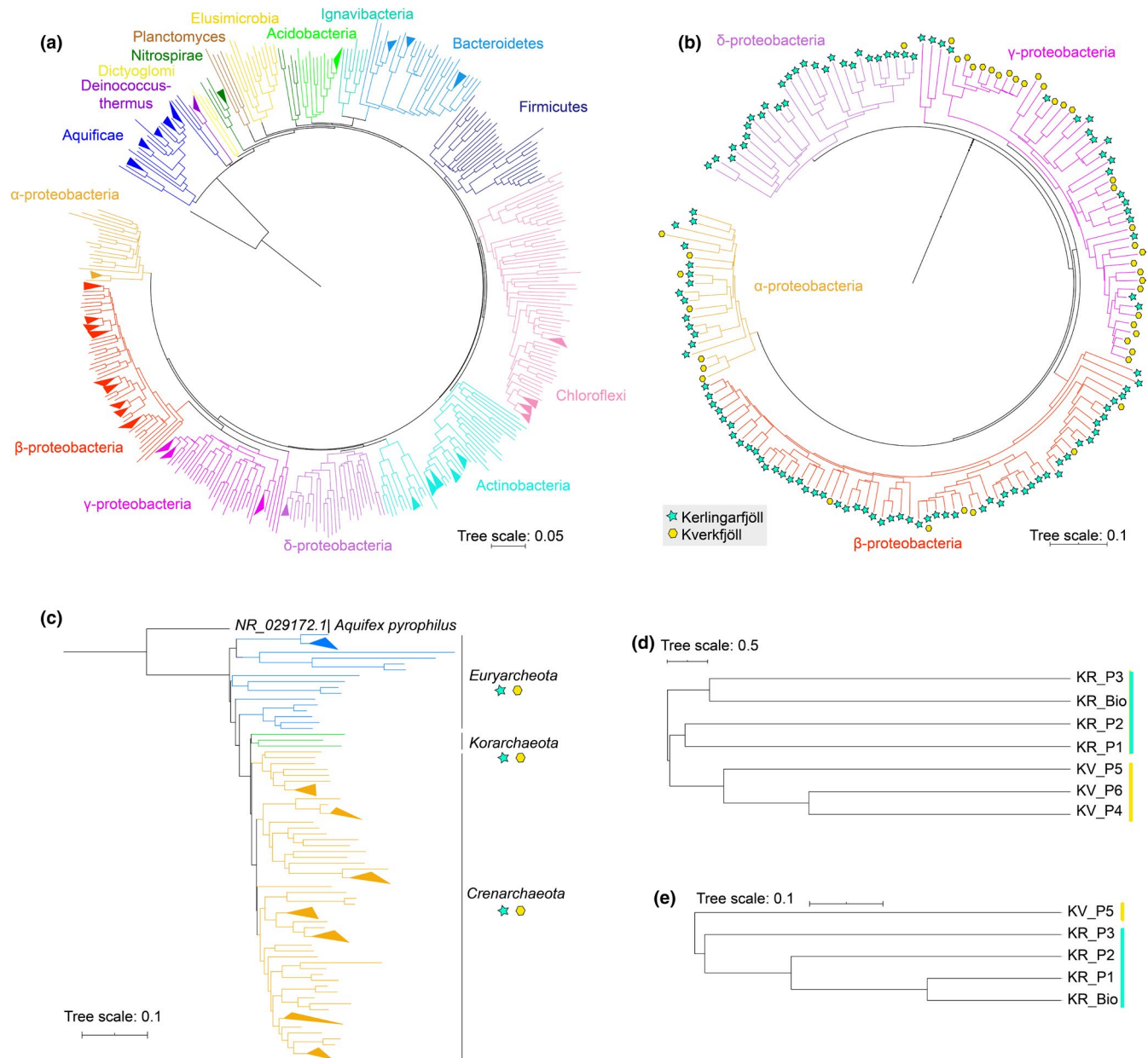


FIGURE 8 (a) Pairwise phylogenetic tree for bacterial OTUs across all sites, with branches <0.04 distance collapsed. Outgroup is *Sulfolobus acidocaldarius* (NR_115499.1). (b) Subtree of Proteobacteria, showing OTUs for both Kerlingarfjöll and Kverkfjöll sites. (c) Pairwise phylogenetic tree for Archaea OTUs across all sites that have archaea present, with branches <0.06 distance collapsed. (d-e) Dendrogram (Yue and Clayton) measure of similarity between bacterial (d) and archaeal (e) community OTUs at Kerlingarfjöll and Kverkfjöll

oxidation. Different types of methanogenesis are potentially operating at Kerlingarfjöll. Hydrogenotrophic methanogenesis dominates at KR-P1 and KR-P3, whereas in KR-P2 sediments acetoclastic methanogenesis dominates. The dominant archaeal metabolic pathways within the KR-Bio community are sulphur respiration (from *Thermofilum*), aerobic ammonia oxidation and nitrification. The dominant bacterial metabolic pathways (Figure 10 and Table S7) identified at Kerlingarfjöll pools KR-P1 and KR-P2 are sulphur oxidation and respiration of sulphate. Dark oxidation of sulphur compounds dominates KR-P3 and KR-Bio. KR-Bio OTUs are associated with both the oxidation of sulphur compounds and molecular hydrogen. Both functional respirations are

carried out by *Sulfurihydrogenibium* (Flores et al., 2008). These results are supported by positive ApSr PCR products for KR-P1, KR-P2, KR-P3 and KR-Bio, identifying the potential of the communities in these pools to undertake sulphate reduction.

The bacterial metabolisms identified within Kverkfjöll pools dominantly involve the oxidation of sulphur and iron species. Pools KV-P4 and KV-P6 present parallel metabolic pathways with dark oxidation of iron being preferred, linked to the presence of *Acidithiobacillus*, *Sulfobacillus* and *Leptospirillum*. Pool KV-P5 shows almost complete cycling of nitrogen coupled with chemoheterotrophy (including



FIGURE 9 Sequence counts of archaeal OTUs associated with different cellular metabolisms (Y axis) obtained with the FAPROTAX database for archaea metabolisms

metabolic paths that oxidise methanol and more complex organic molecules such as aromatic hydrocarbons).

5 | DISCUSSION

5.1 | Volcanic gas and surface water controls on the local environment

The major differences in pH and temperature between Kerlingarfjöll and Kverkfjöll pool chemistries can be explained by acid supply and the ratio of geothermal steam to snowmelt; both are the result of deep

geothermal processes. The geochemistry of the Kerlingarfjöll pools is typical of carbonated waters, with pH between 5 and 7 and high levels of K, Ca and Mg in solution (Björke, 2010; Björke et al., 2015; Kaasalainen & Stefánsson, 2012; Markússon & Stefánsson, 2011). When the CO₂ from volcanic steam mixes with surface waters, it releases a mild acid, dropping the pH < 7 (Björke, 2010). Kverkfjöll pool geochemistry conversely is consistent with acidic SO₄²⁻-rich waters (Markússon & Stefánsson, 2011), with the concentration of SO₄²⁻ and Cl⁻ in surface geothermal waters dependent on depressurisation, boiling and vapour generation in the upwelling fluid (Arnórsson et al., 2007; Giggenbach & Stewart, 1982; Gysi & Stefánsson, 2012; Markússon & Stefánsson, 2011). Here, Cl⁻ is retained in the liquid



FIGURE 10 Sequence counts of bacterial OTUs associated with different cellular metabolisms (Y axis) obtained with the FAPROTAX data base for bacteria metabolism

phase and concentrates underground after boiling, whereas H_2S goes into the vapour phase, encounters oxidising water, condenses and becomes oxidised to H_2SO_4 , producing acidic surface waters with almost undetectable Cl^- and high SO_4^{2-} concentrations (Arnórsson & Andressdottir, 1995; Stefánsson et al., 2016; Figure 3a,b). At both sites, steam mixes with snowmelt, indicated by the similar Cl^- concentrations between the pools (from 0.85 to 2.01 at Kerlingarfjöll, 0.21 to 3.0 ppm at Kverkfjöll) and their respective snowpack values (KR-ice 2.32 ppm and KV-ice 3.97 ppm). This mixing is further evidenced by the low temperatures (16.8–23.6°C) of the pools that are proximal to the glacier and surface snowpack (KR-P1, KR-P2; KV-P4,

KV-P5, KV-P6). Thermal imaging (Figure 2) reveals the spatial association between these thermal end members.

The $\delta^{18}\text{O}$ and δD values of pool waters from both sites also imply condensed steam mixing with surface waters. The isotopic values of pool waters follow an evaporation trajectory with a lower slope for both Kerlingarfjöll (3.5, $R^2 = .7$) and Kverkfjöll (4.2, $R^2 = .9$), compared with the IMWL (Icelandic Meteoric Water Line; 6.5), suggesting the pools underwent different degrees of evaporation (highest for smaller pools KR-P1 and KV-P6, Figure 3d). The origin of the evaporation trajectory for Kerlingarfjöll and Kverkfjöll, estimated from the intersection with the IMWL, differs from the ice-melt values measured and Icelandic rainwaters (MacDonald et al., 2016).

Instead, the Kverkfjöll intersection with the meteoric line is close to the water and steam values measured here by Ólafsson (2000; Figure 3d). This indicates that the source of water for the pools is isotopically depleted compared with the meteoric input, with additional contribution by steam condensation from boiling groundwater at depth, which has more negative $\delta^{18}\text{O}$ and δD (Ólafsson et al., 2000). No steam values have been measured at Kerlingarfjöll, but the similarity of the Kerlingarfjöll trend to the Kverkfjöll trend indicates a comparable process.

5.2 | Water–rock interaction and alteration mineralogy

Phase segregation of geothermal aquifer fluids (the separation of a volatile-enriched vapour phase during subsurface boiling) upon ascent to the surface affects acid supply, which in turn drives bedrock leaching (Kaasalainen & Stefansson, 2012). This process explains differences in ion concentrations between sites. The Kverkfjöll pools KV-P5 and KV-P6 have an extremely low pH (1.7–2.7) and the highest total ion concentrations (Figure 3), whereas the circum-neutral Kerlingarfjöll pools show lower dissolved ion concentrations. A low ion concentration in Kverkfjöll pool KV-P4 is likely due to dilution by the observed influx and outflow of meltwater. The mineral alteration assemblages are largely specific to their immediate pool environments, with no assemblage consistently representing either basalt- or rhyolite-hosted pools. Instead, phases are locally controlled by (i) acid supply, (ii) the intensity of the surface hydrothermal activity and temperature and (iii) the ratio of geothermal steam to meteoric water. All of these result from geothermal activity rather than host lithology (Markússon & Stefánsson, 2011).

A geothermal control on alteration mineralogy is also supported by the elemental geochemistry results. Both Kerlingarfjöll and Kverkfjöll sediments are depleted in SiO_2 and $\text{Na}_2\text{O}+\text{K}_2\text{O}$ compared with their host rocks and enriched Al_2O_3 and TiO_2 , indicative of hydrothermal alteration (Markússon & Stefánsson, 2011). CIA values of authigenic phases further indicate high levels of chemical alteration compared with the volcanic host rock. An exception to this pattern is the quartz identified within the low temperature ($\sim 20^\circ\text{C}$) Kerlingarfjöll pools KR-P1 and KR-P2. Given the temperatures of these pools, this is the only phase that attests to an origin within a felsic host lithology, as it is likely detrital, weathered directly from surrounding quartz-bearing bedrock. Alternatively, it could be derived via higher-temperature hydrothermal remobilisation of Si and subsequent mineralisation. Given the hydrothermal nature of the alteration environment, it is also likely that there are amorphous Si phases present, but not detectable with XRD.

5.3 | S and Fe redox chemistry of the pools

The Eh–pH diagrams help to further resolve the S and Fe redox chemistry of the pools. The sulphur results indicate SO_4^{2-} being

the stable form in Kerlingarfjöll and FeSO_4^0 in Kverkfjöll, which is consistent with the high SO_4^{2-} concentrations measured at both sites. The results show Fe contained in fluids from Kerlingarfjöll has undergone more extensive oxidation compared to Kverkfjöll. Importantly, the degree of Fe oxidation is not only dependent on dissolved oxygen availability but also a function of pH. As the pH is higher at the Kerlingarfjöll site, the thermodynamic redox boundary between Fe^{2+} and Fe^{3+} is lower, allowing oxidation to go to completion even at relatively low concentrations of dissolved oxygen. Since Kerlingarfjöll is rhyolite-hosted, the initial Fe endowment of the fluid is likely lower compared to the basalt-hosted site at Kverkfjöll. However, a higher degree of oxidation may have further lowered the total dissolved Fe concentrations at Kerlingarfjöll, as the fluids have been pushed well into the stability field of hematite, likely causing Fe precipitation (Figures 4 and S4). This leads to Kerlingarfjöll having almost no dissolved Fe available for microbial cycling. In contrast, the samples from Kverkfjöll contain a high proportion of reduced iron (paired with some dissolved oxygen), sufficient to support an active community of Fe^{2+} -oxidising microbes, as confirmed by the DNA results (Figure 10). Microbially oxidised iron would likely initially precipitate as amorphous hydroxides and later dehydrate into hematite (Fischer & Schwertmann, 1975). Occurrences of hematite at Kverkfjöll noted by Cousins et al., (2013) could be evidence of such microbial activity. In the current study, pyrite dominated sediment XRD data, despite the fluids falling in the hematite stability field (Figure 4d). This may indicate that the ferric iron in these sediments has not yet ‘matured’ into hematite, which typically requires dehydration of amorphous ferric hydroxide phases (Fischer & Schwertmann, 1975). The presence of pyrite indicates a strong thermodynamic disequilibrium between the fluid that is exposed to the atmosphere and the underlying sediments. This disequilibrium is likely a key driver of the biological metabolisms present in the pools.

5.4 | Volcanic controls on microbial communities

The deep volcanic processes discussed above control which microbial groups and associated metabolisms are supported by the local geochemistry, by defining local pH and the bioavailability of electron donors and acceptors through speciation of S and Fe. For example, the volcanic processes operating at Kerlingarfjöll and Kverkfjöll result in a predominance of SO_4^{2-} in the resulting hydrothermal pools at both sites, which in turn facilitates a dominance of sulphur-driven redox metabolisms. This control is broadly consistent with previous observations at Yellowstone National Park, USA (Colman et al., 2016, 2019).

At Kverkfjöll, acidic pools are dominated by the strong acid released when H_2S is oxidised to SO_4^{2-} . In hydrothermal acidic waters, Fe is more soluble, with the relative distribution of $\text{Fe}^{2+}/\text{Fe}^{3+}$ controlled by a combination of the underlying basaltic bedrock, Fe^{2+} oxidation kinetics and microbial Fe cycling (Kaasalainen et al., 2017). At Kverkfjöll pools, the Eh–pH diagrams show Fe^{2+} as the most abundant species in solution, forming a FeSO_4^0 ion pair, or free Fe^{2+} at

KV-P4. The Fe^{2+} available in solution allows the dominance of Fe-cycling bacterial taxa in the pool sediments at this site, including *Sulfobacillus*, *Acidithiobacillus*, *Ferrimicrobium* and *Acidobacter*. These bacteria can perform both dark iron oxidation and dark sulphur oxidation (Coupland et al., 2008; Druschel et al., 2004). At the same time, they could be contributing to the high concentrations of SO_4^{2-} and Fe (e.g. KV-P6) and maintaining the low pH of the pools by oxidising sulphur and iron (Colman et al., 2019); both sulphide/sulphur and Fe^{2+} oxidation are H^+ -producing reactions that stabilise at low pH. At low pH, sulphate respiration and methanogenesis are typically inhibited when they are amongst the presence of very electropositive electron acceptors, such as Fe^{3+} (Sánchez-Andrea et al., 2011; Bodegom et al., 2004). The confirmed presence of iron oxidising bacteria, together with the field observations of red water colouration for KV-P6 (Figure 1h), likely indicates that although the dominant aqueous Fe species is in a +2 state, aqueous Fe^{3+} is present in the pools, produced, at least in part, by iron oxidising microorganisms.

By contrast, the circum-neutral Kerlingarfjöll pools, present aqueous CO_2 delivered by volcanic gases which produces moderate pH and likely drives archaeal methanogenesis. The Fe in Kerlingarfjöll pools is undetectable, likely due to pervasive precipitation of hematite and other Fe^{3+} mineral phases. The biological Fe cycle is therefore limited, allowing sulphate respiration to be the principal metabolism (Sánchez-Andrea et al., 2011). *Sulfurihydrogenibium* dominates at KR-Bio and likely performs dark oxidation of sulphur compounds and molecular hydrogen (Figure 10). It also has been identified in other Icelandic hydrothermal locations (Flores et al., 2008) and at Mammoth Hot Spring, Yellowstone National Park, USA (Dong et al., 2019). *Sulfurihydrogenibium* is an evolutionarily primitive taxon often found dominating filamentous microbial mat communities in shallow fast flowing aqueous systems globally (Dong et al., 2019).

This pH control can also be observed in the diversity of the archaeal phylogenetic structure from Kerlingarfjöll pools and Kverkfjöll KV-P5. The archaeal communities from Kerlingarfjöll are more diverse than Kverkfjöll KV-P5 (Figure 7b) as the conditions are not so extreme: the pH is near neutral, and there are CO_2 and anoxic conditions, which permit abundant methanogenesis. On the other hand, KV-P5 is dominated by acidophilic-thermophilic archaea. Although the archaeal phylogenetic structures between sites are very different (Figure 8e), some of the archaeal communities are shared (Figure 7b and Figure 8c). This relation potentially reflects the wide range of pH for growth of the identified archaeal taxa, such as *Candidatus Nitrosocaldus* (pH 3–7.5; Abby et al., 2018; Jung et al., 2014) and *Aciduliprofundum* (pH 3–5.8; Reysenbach et al., 2006; Schouten et al., 2008).

A stronger pH and temperature control is imparted on the bacterial communities at Kerlingarfjöll and Kverkfjöll (Figure 8d). The structural differences in bacterial community are dictated first by pH (Kerlingarfjöll versus Kverkfjöll) and then temperature (high-temperature KR-P3 and KR-Bio; low-temperature KR-P1, and KR-P2 within Kerlingarfjöll, and Kverkfjöll pools). The temperatures of the individual pools are regulated by the input of melted ice from the glacier and snowmelt into the pools. The mild temperatures

from Kerlingarfjöll KR-P1, KR-P2 and Kverkfjöll pools define a bacterial community dominated by mesophilic phylum Proteobacteria. Instead, KR-P3 and KR-Bio pools, which present higher temperatures (60–70°C), are dominated by thermophilic Aquificae groups.

5.5 | Implications for the habitability of past Martian hydrothermal environments

Icelandic hot springs such as Kerlingarfjöll and Kverkfjöll provide a useful example of how hydrothermal systems are a localised source of metabolic redox pairs for chemolithotrophic microorganisms and accessible trace metals (e.g. Cr, Mn, Zn) leached from the bedrock. These redox pairs and trace metals are fundamental for microbial metabolism (Havig et al., 2015; Kee et al., 2013) and potentially prebiotic chemistry (Rimmer & Shortle, 2019). Acid supply and surface activity resulting from deep volcanic processes and redox conditions create two distinct geochemical environments that are largely independent of bedrock lithology. The interaction between steam and gas from volcanic fumaroles and meteoric surface water-ice results in liquid water of unusually moderate temperatures for hydrothermal systems (around 16–20°C). Where these types of ice-fed hydrothermal systems existed on early Mars (e.g. Sisyphi Montes and Arsia Mons), similar processes would likely operate. Such hydrothermal volcanic environments on Mars could have maintained locally independent anoxic conditions and circum-neutral pH through the delivery of reduced volcanic gases, even when surface conditions on Mars became more oxidised. Subsequently, hydrothermal sites would present an important habitability advantage compared with non-volcanic systems, locally isolating the habitat from Mars's oxidising atmospheric conditions. Sedimentary mineral alteration assemblages are also controlled by the volcanic system at a small scale and thus record a signature of the pH and major metabolic substrates (Fe, S) available for microorganisms. Such assemblages may persist long after the hydrothermal system ceases activity. Recognition of sedimentary mineral alteration assemblages, however, presents challenges. The mineralogy found here (quartz, kaolinite, smectites, anatase, pyrite) differs from those identified on Mars as resulting from hydrothermalism; for example, from the mineralogy of Sisyphi Montes and Home Plate (opaline silica, sulphates, smectites, palagonite), but also from the study done in Kverkfjöll by Cousins et al., (2013) where gypsum, jarosite, pyrite, iron oxides, smectites and palagonite were found. This discrepancy in mineralogy can be explained with two points. Firstly, Kerlingarfjöll and Kverkfjöll hydrothermal systems present large mineralogical variations across a small scale. In this study, within pools from the same sites, inter-pool mineralogical differences can be observed even though the separation between the pools is <5 m. This demonstrates how the mineralogy from volcanic environments can be highly variable within a localised area and exposes a potential for a poor agreement between small-scale studies and large-scale orbital observations on Mars. Secondly, the samples here were taken from wet sediments at the

sediment–water interface. Mineral species such as the sulphate evaporites observed by Cousins et al., (2013) may form once the sediments dry and are likely precipitating above the water line at the rims of the Kerlingarfjöll and Kverkfjöll pools, as water SO_4^{2-} concentrations are very high (up to 21,000.01 ppm).

On Mars, the widespread presence of S and Fe phases on the surface suggests S and Fe-driven metabolisms could once have been plausible in Martian hydrothermal systems by exploiting redox pairs for energy (Grotzinger et al., 2014; Nixon et al., 2013; Skok et al., 2010). The pools investigated here imply geothermally derived pH limitations on these metabolisms by dictating the bioavailability of Fe or S phases. For circum-neutral-alkaline environments, Fe-driven metabolisms face challenges due to pH-driven precipitation of Fe, while in acidic environments, sulphate respiration and methanogenesis can be inhibited. Furthermore, Fe^{2+} oxidation could be challenging in acidic conditions on Mars, as it is limited to circum-neutral waters and restricted to using nitrate as an electron acceptor (Price et al., 2018). Iron reduction-based metabolisms could alternatively use S^0 as an electron acceptor, with H_2 as an electron donor under anaerobic conditions, with Fe^{3+} as the final electron acceptor (Lovley & Phillips, 1988; Lovley et al., 1989; Price et al., 2018). Consequently, Martian circum-neutral pH hydrothermal environments could have been dominated by methanogenesis, sulphate respiration and sulphur oxidation. Metabolisms dominating acidic hydrothermal environments would be sulphur oxidation, and potentially sulphate respiration, iron oxidation/reduction and nitrate respiration. Overall, our results suggest that sulphur-driven redox metabolisms are the most plausible across different pH environments, as both volcanic systems investigated bear hydrothermal pools with sulphur available for sulphate respiration and sulphur oxidation using either CO_2 or H_2 , consistent with findings from other Mars relevant environments (Macey et al., 2020).

This volcanically driven limitation on feasible microbial metabolisms has wider implications for the detection of resulting microbial biosignatures, particularly those that utilise stable isotope fractionations to distinguish between abiotic from biological processes. Sulphate respiration in particular can produce variable carbon and sulphur stable isotope fractionation values (Johnston et al., 2007; Zerkle et al., 2005, 2016) and are measurable at the Martian surface using current rover-based instruments. Such sulphur stable isotope values will ultimately be recorded within the inorganic sulphur-bearing mineral phases present within the sediments, which at both Kverkfjöll and Kerlingarfjöll are exclusively pyrite. The sample analysis at Mars instrument onboard the NASA MSL Curiosity rover has measured sulphur isotope compositions in Gale crater sediments, with $\delta^{34}\text{S}$ values from Fe-sulphides varying between -47‰ and $+28\text{‰}$, attributed to sulphate-sulphide equilibrium fractionation within a long-term hydrothermal system (Franz et al., 2017). It is therefore of particular importance to use analogue sites such as Kerlingarfjöll and Kverkfjöll to constrain how $\delta^{34}\text{S}$ biosignatures would manifest within relict Martian hydrothermal systems, and how these can be differentiated from abiotic signatures, particularly once the environment becomes inactive.

6 | CONCLUSION

We investigated the geochemical environments and microbial communities within hydrothermal pools at the rhyolitic Kerlingarfjöll volcano and basaltic Kverkfjöll volcano in Iceland. The primary controls on dissolved ion chemistry are acid supply, redox conditions and secondary mineral solubility, with underlying lithology playing a minor role in the precipitation of authigenic phases. Due to the difference in these deep volcanic processes, Kerlingarfjöll and Kverkfjöll hydrothermal pools have distinct geochemical properties, including different water pH (circum-neutral versus acidic).

The resulting microbial communities are controlled by these deep volcanic processes in addition to thermal regulation by surface snow and ice input, determining the availability of electron donors and acceptors for metabolism and the temperatures of the pools. Consequently, Kerlingarfjöll sites are dominated by methanogens, sulphate reducers and S oxidisers, whereas the Kverkfjöll microbial communities are dominated by microorganisms utilising S oxidation and Fe oxidation, which themselves will impart different geochemical biosignatures.

This study demonstrates how hydrothermal pools are relevant for understanding past Martian hydrothermal environments on a small scale and that local volcanic inputs can strongly affect microbial community function, with implications for the feasibility of geochemical biosignatures that can be preserved within the geological record.









ACKNOWLEDGMENTS

This work was funded by a UK Space Agency PhD Studentship (ST/P001270/1) to C Cousins and A Zerkle, and a Europlanet 2017 TA1 facility grant 'Planetary Field Analogue Sites (PFA)' and Earth and Space Foundation grant, both to A Moreras-Marti. Research, access and sample export permits were granted by Orkustofnun (Reference OS2016120056/50.44), and we thank Vatnajökulsþjóðgarður for sampling permission, and the Icelandic Institute of Natural History for the sample export licence. Dr. Fernando Gázquez was financially supported by the 'HIPATIA' research program of the University of Almeria. Finally, we thank Elyse Allender and Matthew Gunn for fieldwork assistance in Iceland, and Matthias Vogt (Volcano-Heli) for logistical support at Kverkfjöll. Part of this research was carried out on the Powder diffraction beamline at the Australian Synchrotron.

DATA AVAILABILITY STATEMENT

The data that support the findings of this study are available from the corresponding author upon reasonable request.

ORCID

Arola Moreras-Marti  <https://orcid.org/0000-0002-6204-7213>
 Mark Fox-Powell  <https://orcid.org/0000-0002-4994-5203>
 Aubrey L. Zerkle  <https://orcid.org/0000-0003-2324-1619>
 Eva Stueeken  <https://orcid.org/0000-0001-6861-2490>
 Fernando Gázquez  <https://orcid.org/0000-0001-8258-1352>
 Helen E. A. Brand  <https://orcid.org/0000-0002-7217-171X>
 Lotta Purkamo  <https://orcid.org/0000-0002-9428-6542>
 Claire R. Cousins  <https://orcid.org/0000-0002-3954-8079>

REFERENCES

- Abby, S. S., Melcher, M., Kerou, M., Krupovic, M., Stieglmeier, M., Rossel, C., Pfeifer, K., & Schleper, C. (2018). Candidatus Nitrosocaldus cavascurensis, an ammonia oxidizing, extremely thermophilic archaeon with a highly mobile genome. *Frontiers in Microbiology*, 9, 28. <https://doi.org/10.3389/fmicb.2018.00028>
- Ackiss, S., Horgan, B., Seelos, F., Farrand, W., & Wray, J. (2018). Mineralogic evidence for subglacial volcanism in the Sisyphi Montes region of Mars. *Icarus*, 311, 357–370. <https://doi.org/10.1016/j.icarus.2018.03.026>
- Ackiss, S., Horgan, B., Suda, M., Minton, D., & Campbell, A. (2019). Geomorphologic mapping of a possible Hesperian subglacial volcanic environment in the Sisyphi Montes, Mars. 50th Lunar and Planetary Science Conference 2019 (LPI Contrib. No. 2132).
- Ármansson, H. (2016). The fluid geochemistry of Icelandic high temperature geothermal areas. *Applied Geochemistry*, 66, 14–64. <https://doi.org/10.1016/j.apgeochem.2015.10.008>
- Arnósson, S., & Andresdóttir, A. (1995). Processes controlling the distribution of boron and chlorine in natural-waters in Iceland. *Geochimica et Cosmochimica Acta*, 59(20), 4125–4146. [https://doi.org/10.1016/0016-7037\(95\)00278-8](https://doi.org/10.1016/0016-7037(95)00278-8)
- Arnósson, S., Stefánsson, A., & Bjarnason, J. Ö. (2007). Fluid-fluid interactions in geothermal systems. *Reviews in Mineralogy and Geochemistry*, 65(1), 259–312. <https://doi.org/10.2138/rmg.2007.65.9>
- Bethke, C. (2011). *The Geochemist's workbench software package (version 9.0)*. University of Illinois.
- Björke, J. K. (2010). *Fluid-rhyolite interaction in geothermal systems, Torfajökull Iceland - secondary surface mineralogy and fluid chemistry upon phase segregation and fluid mixing*. Master's thesis, Faculty of Earth Sciences, University of Iceland, p. 61.
- Björke, J. K., Stefánsson, A., & Arnósson, S. (2015). Surface water chemistry at Torfajökull, Iceland-Quantification of boiling, mixing, oxidation and water-rock interaction and reconstruction of reservoir fluid composition. *Geothermics*, 58, 75–86. <https://doi.org/10.1016/j.geothermics.2015.09.007>
- Björnsson, H., & Pálsson, F. (2008). Icelandic glaciers. *Jökull*, 58, 365–386.
- Cassanelli, J. P., & Head, J. W. (2019). Glaciovolcanism in the Tharsis volcanic province of Mars: Implications for regional geology and hydrology. *Planetary and Space Science*, 169, 45–69. <https://doi.org/10.1016/j.pss.2019.02.006>
- Chapman, M. G., Allen, C. C., Gudmundsson, M. T., Gulick, V. C., Jakobsson, S. P., Lucchitta, B. K., Waitt, R. B. (2000). Volcanism and ice interactions on Earth and Mars. In *Environmental effects on volcanic eruptions* (pp. 39–73). Springer.
- Cline, J. D. (1969). Spectrophotometric determination of hydrogen sulfide in natural waters 1. *Limnology and Oceanography*, 14(3), 454–458.
- Cockell, C. S., & Lee, P. (2002). The biology of impact craters - A review. *Biological Reviews of the Cambridge Philosophical Society*, 77(3), 279–310. <https://doi.org/10.1017/S146479310100584X>
- Colman, D. R., Feyhl-Buska, J., Robinson, K. J., Fecteau, K. M., Xu, H., Shock, E. L., & Boyd, E. S. (2016). Ecological differentiation in planktonic and sediment-associated chemotrophic microbial populations in Yellowstone hot springs. *FEMS Microbiology Ecology*, 92(9), fiw137. <https://doi.org/10.1093/femsec/fiw137>
- Colman, D. R., Lindsay, M. R., & Boyd, E. S. (2019). Mixing of meteoric and geothermal fluids supports hyperdiverse chemosynthetic hydrothermal communities. *Nature Communications*, 10(1), 1–13. <https://doi.org/10.1038/s41467-019-08499-1>
- Coupland, K., & Johnson, D. B. (2008). Evidence that the potential for dissimilatory ferric iron reduction is widespread among acidophilic heterotrophic bacteria. *FEMS Microbiology Letters*, 279(1), 30–35. <https://doi.org/10.1111/j.1574-6968.2007.00998.x>
- Cousins, C. (2015). Volcanogenic fluvial-lacustrine environments in Iceland and their utility for identifying past habitability on Mars. *Life*, 5, 568–586. <https://doi.org/10.3390/life5010568>
- Cousins, C. R., & Crawford, I. A. (2011). Volcano-Ice interaction as a microbial habitat on Earth and Mars. *Astrobiology*, 11(7), 695–710. <https://doi.org/10.1089/ast.2010.0550>
- Cousins, C. R., Crawford, I. A., Carrivick, J. L., Gunn, M., Harris, J., Kee, T. P., Karlsson, M., Carmody, L., Cockell, C., Herschy, B., & Joy, K. H. (2013). Glaciovolcanic hydrothermal environments in Iceland and implications for their detection on Mars. *Journal of Volcanology and Geothermal Research*, 256, 61–77. <https://doi.org/10.1016/j.jvolgeores.2013.02.009>
- Cousins, C. R., Fogel, M., Bowden, R., Crawford, I., Boyce, A., Cockell, C., & Gunn, M. (2018). Biogeochemical probing of microbial communities in a basalt-hosted hot spring at Kverkfjöll volcano. *Iceland. Geobiology*, 16(5), 507–521. <https://doi.org/10.1016/j.icarus.2018.03.026>
- DeLong, E. F. (1992). Archaea in coastal marine environments. *Proceedings of the National Academy of Sciences of the United States of America*, 89(12), 5685–5689. <https://doi.org/10.1073/pnas.89.12.5685>
- Direito, S. O., Marees, A., & Röling, W. F. (2012). Sensitive life detection strategies for low-biomass environments: Optimizing extraction of nucleic acids adsorbing to terrestrial and Mars analogue minerals. *FEMS Microbiology Ecology*, 81(1), 111–123.
- Dong, Y., Sanford, R. A., Inskeep, W. P., Srivastava, V., Bulone, V., Fields, C. J., Yau, P. M., Sivaguru, M., Ahrén, D., Fouke, K. W., Weber, J., Werth, C. R., Cann, I. K., Keating, K. M., Khetani, R. S., Hernandez, A. G., Wright, C., Band, M., Imai, B. S., ... Fouke, B. W. (2019). Physiology, metabolism, and fossilization of hot-spring filamentous microbial mats. *Astrobiology*, 19(12), 1442–1458. <https://doi.org/10.1089/ast.2018.1965>
- Druschel, G. K., Baker, B. J., Gihring, T. M., & Banfield, J. F. (2004). Acid mine drainage biogeochemistry at Iron Mountain. *California. Geochemical Transactions*, 5(2), 13. <https://doi.org/10.1186/1467-4866-5-13>
- Ehlmann, B. L., Mustard, J. F., Murchie, S. L., Bribing, J. P., Meunier, A., Fraeman, A. A., & Langevin, Y. (2011). Subsurface water and clay mineral formation during the early history of Mars. *Nature*, 479, 53–60. <https://doi.org/10.1038/nature10582>
- Fischer, W. R., & Schwertmann, U. (1975). The formation of hematite from amorphous iron (III) hydroxide. *Clays and Clay Minerals*, 23(1), 33–37. <https://doi.org/10.1346/CCMN.1975.0230105>
- Flores, G. E., Liu, Y., Ferrera, I., Beveridge, T. J., & Reysenbach, A. L. (2008). Sulfurihydrogenibium kristjanssonii sp. nov., a hydrogen- and sulfur-oxidizing thermophile isolated from a terrestrial Icelandic hot spring. *International Journal of Systematic and Evolutionary Microbiology*, 58(5), 1153–1158.
- Flude, S., McGarvie, D. W., Burgess, R., & Tindle, A. G. (2010). Rhyolites at Kerlingarfjöll, Iceland: The evolution and lifespan of silicic central volcanoes. *Bulletin of Volcanology*, 72(5), 523–538. <https://doi.org/10.1007/s00445-010-0344-0>
- Franz, H. B., McAdam, A. C., Ming, D. W., Freissinet, C., Mahaffy, P. R., Eldridge, D. L., Fischer, W. W., Grotzinger, J. P., House, C. H., Hurowitz, J. A., McLennan, S. M., Schwenzer, S. P., Vaniman, D. T., Archer Jr, P. D., Atreya, S. K., Conrad, P. G., Drottin, J. W. III, Eigenbrode, J. L., Farley, K. A., ... Sutter, B. (2017). Large sulfur isotope fractionations in Martian sediments at Gale crater. *Nature Geoscience*, 10(9), 658–662. <https://doi.org/10.1038/ngeo3002>
- Friedrich, M. W. (2002). Phylogenetic analysis reveals multiple lateral transfers of adenosine-5'-phosphosulfate reductase genes among sulfate-reducing microorganisms. *Journal of Bacteriology*, 184(1), 278–289. <https://doi.org/10.1128/JB.184.1.278-289.2002>
- Gaidos, E., & Marion, G. (2003). Geological and geochemical legacy of a cold early Mars. *Journal of Geophysical Research*, 108(E6), 5055. <https://doi.org/10.1029/2002JE002000>
- Gaidos, E., Marteinsson, V., Thorsteinsson, T., Jóhannesson, T., Rúnarsson, Á. R., Stefansson, A., Glazer, B., Lanoil, B., Skidmore, M., Han, S., Miller, M., Rusch, A., & Foo, W. (2009). An oligarchic microbial assemblage in the anoxic bottom waters of a volcanic subglacial lake. *The ISME Journal*, 3(4), 486–497. <https://doi.org/10.1038/ismej.2008.124>

- Giggenbach, W. F., & Stewart, M. K. (1982). Processes controlling the isotopic composition of steam and water discharges from steam vents and steam-heated pools in geothermal areas. *Geothermics*, 11(2), 71–80. [https://doi.org/10.1016/0375-6505\(82\)90009-8](https://doi.org/10.1016/0375-6505(82)90009-8)
- Grönvold, K. (1972). *Structural and petrochemical studies in the Kerlingarfjöll region, central Iceland*. Ph.D. thesis, University of Oxford.
- Grotzinger, J. P., Sumner, D. Y., Kah, L. C., Stack, K., Gupta, S., Edgar, L., Rubin, D., Lewis, K., Schieber, J., Mangold, N., Milliken, R., Conrad, P. G., DesMarais, D., Farmer, J., Siebach, K., Calef, F., Hurowitz, J., McLennan, S. M., Ming, D., ... Moores, J. E. (2014). A habitable fluvio-lacustrine environment at Yellowknife Bay, Gale Crater, Mars. *Science*, 343(6169), 1242777. <https://doi.org/10.1126/science.1242777>
- Gudmundsson, A. (2000). Dynamics of volcanic systems in Iceland: Example of tectonism and volcanism at juxtaposed hot spot and mid-ocean ridge systems. *Annual Review of Earth and Planetary Sciences*, 28(1), 107–140. <https://doi.org/10.1146/annurev.earth.28.1.107>
- Gysi, A. P., & Stefánsson, A. (2012). CO₂-water-basalt interaction. Low temperature experiments and implications for CO₂ sequestration into basalts. *Geochimica et Cosmochimica Acta*, 81, 129–152. <https://doi.org/10.1016/j.gca.2011.12.012>
- Havig, J. R., McCormick, M. L., Hamilton, T. L., & Kump, L. R. (2015). The behavior of biologically important trace elements across the oxic/euxinic transition of meromictic Fayetteville Green Lake, New York, USA. *Geochimica et Cosmochimica Acta*, 165, 389–406. <https://doi.org/10.1016/j.gca.2015.06.024>
- Havig, J. R., Raymond, J., Meyer-Dombard, D. A. R., Zolotova, N., & Shock, E. L. (2011). Merging isotopes and community genomics in a siliceous sinter-depositing hot spring. *Journal of Geophysical Research*, 116, G01005. <https://doi.org/10.1029/2010JG001415>
- Hays, L. E., Graham, H. V., Des Marais, D. J., Hausrath, E. M., Horgan, B., McCollom, T. M., Parenteau, M. N., Potter-McIntyre, S. L., Williams, A. J., & Lynch, K. L. (2017). Biosignature preservation and detection in Mars analog environments. *Astrobiology*, 17(4), 1–38. <https://doi.org/10.1089/ast.2016.1627>
- Head, J. W., & Wilson, L. (2007). Heat transfer in volcano–ice interactions on Mars: Synthesis of environments and implications for processes and landforms. *Annals of Glaciology*, 45, 1–13.
- Hiesinger, H., & Head, J. W. III (2004). The Syrtis Major volcanic province, Mars: Synthesis from Mars global surveyor data. *Journal of Geophysical Research: Planets*, 109(E1), E01004.
- Humlum, J. (1936). Hveradalir in Kerlingarfjöll, Iceland. *Geografisk Tidsskrift*, 11–34.
- Hurowitz, J. A., McLennan, S. M., Tosca, N. J., Arvidson, R. E., Michalski, J. R., Ming, D. W., Schröder, C., & Squyres, S. W. (2006). In situ and experimental evidence for acidic weathering of rocks and soils on Mars. *Journal of Geophysical Research*, 111, E02S19. <https://doi.org/10.1029/2005JE002515>
- Jakobsson, S. P., Jónasson, K., & Sigurdsson, I. A. (2008). The three igneous rock series of Iceland. *Jökull*, 58, 117–138.
- Johnston, D. T., Farquhar, J., & Canfield, D. E. (2007). Sulfur isotope insights into microbial sulfate reduction: When microbes meet models. *Geochimica et Cosmochimica Acta*, 71(16), 3929–3947. <https://doi.org/10.1016/j.gca.2007.05.008>
- Jung, M. Y., Park, S. J., Kim, S. J., Kim, J. G., Damsté, J. S. S., Jeon, C. O., & Rhee, S. K. (2014). A mesophilic, autotrophic, ammonia-oxidizing archaeon of thaumarchaeal group I. 1a cultivated from a deep oligotrophic soil horizon. *Applied and Environment Microbiology*, 80(12), 3645–3655.
- Kaasalainen, H., & Stefánsson, A. (2012). The chemistry of trace elements in surface geothermal waters and steam, Iceland. *Chemical Geology*, 330–331, 60–85. <https://doi.org/10.1016/j.chemgeo.2012.08.019>
- Kaasalainen, H., Stefánsson, A., & Druschel, G. K. (2017). Geochemistry and speciation of Fe(II) and Fe(III) in natural geothermal water, Iceland. *Applied Geochemistry*, 87(October), 146–157. <https://doi.org/10.1016/j.apgeochem.2017.10.021>
- Kee, T., Bryant, D., Herschy, B., Marriott, K., Cosgrove, N., Pasek, M., Atlas, Z., & Cousins, C. (2013). Phosphate activation via reduced oxidation state phosphorus (P). mild routes to condensed-P energy currency molecules. *Life*, 3(3), 386–402. <https://doi.org/10.3390/life3030386>
- Letunic, I., & Bork, P. (2019). Interactive Tree Of Life (iTOL) v4: Recent updates and new developments. *Nucleic Acids Research*, 47(W1), W256–W259. <https://doi.org/10.1093/nar/gkz239>
- Louca, S., Parfrey, L. W., & Doebeli, M. (2016). Decoupling function and taxonomy in the global ocean microbiome. *Science*, 353(6305), 1272–1277.
- Lovley, D. R., & Phillips, E. J. (1988). Novel mode of microbial energy metabolism: Organic carbon oxidation coupled to dissimilatory reduction of iron or manganese. *Applied and Environmental Microbiology*, 54(6), 1472–1480. <https://doi.org/10.1128/aem.54.6.1472-1480.1988>
- Lovley, D. R., Phillips, E. J., & Lonergan, D. J. (1989). Hydrogen and formate oxidation coupled to dissimilatory reduction of iron or manganese by *Alteromonas putrefaciens*. *Applied and Environmental Microbiology*, 55(3), 700–706.
- MacDonald, A. M., Black, A. R., Ó Dochartaigh, B. é., Everest, J., Darling, W. G., Flett, V., & Peach, D. W. (2016). Using stable isotopes and continuous meltwater river monitoring to investigate the hydrology of a rapidly retreating Icelandic outlet glacier. *Annals of Glaciology*, 57(72), 151–158. <https://doi.org/10.1017/aog.2016.22>
- Macey, M. C., Fox-Powell, M., Ramkissoon, N. K., Stephens, B. P., Barton, T., Schwenzer, S. P., Pearson, V. K., Cousins, C. R., & Olsson-Francis, K. (2020). The identification of sulfide oxidation as a potential metabolism driving primary production on late Noachian Mars. *Scientific Reports*, 10(1), 1–13.
- Markússon, S. H., & Stefánsson, A. (2011). Geothermal surface alteration of basalts, Krýsuvík Iceland-Alteration mineralogy, water chemistry and the effects of acid supply on the alteration process. *Journal of Volcanology and Geothermal Research*, 206(1–2), 46–59. <https://doi.org/10.1016/j.jvolgeores.2011.05.007>
- Michalski, J. R., Noe Fobrea, E. Z., Niles, P. B., & Cuadros, J. (2017). Ancient hydrothermal seafloor deposits in Eridania basin on Mars. *Nature Communications*, 8, 15978. <https://doi.org/10.1038/ncomm515978>
- Ming, D. W., Gellert, R., Morris, R. V., Arvidson, R. E., Brueckner, J., Clark, B. C., Cohen, B. A., d'Ulston, C., Economou, T., Fleicher, I., Klingelhoefer, G., McCoy, T. J., Mittlefehldt, D. W., Schmidt, M. E., Schroder, C., Squyres, S. W., Treguier, E., Yen, A. S., & Zipfel, J. (2008). Geochemical properties of rocks and soils in Gusev crater, Mars: Results of the Alpha Particle X-Ray spectrometer from Cumberland Ridge to Home Plate. *Journal of Geophysical Research*, 113, E12S39. <https://doi.org/10.1029/2008JE003195>
- Nesbitt, H. W., & Young, G. M. (1982). Early Proterozoic climates and plate motions inferred from major element chemistry of lutites. *Nature*, 299, 715–717. <https://doi.org/10.1038/299715a0>
- Nesbitt, H. W., & Young, G. M. (1984). Prediction of some weathering trends of plutonic and volcanic rocks based on thermodynamic and kinetic considerations. *Geochimica Et Cosmochimica Acta*, 48, 1523–1534. [https://doi.org/10.1016/0016-7037\(84\)90408-3](https://doi.org/10.1016/0016-7037(84)90408-3)
- Nicholson, H., & Latin, D. (1992). Olivine Tholeiites from Krafla, Iceland: Evidence for variations in melt fraction within a plume. *Journal of Petrology*, 33(5), 1105–1124. <https://doi.org/10.1093/ptrology/33.5.1105>
- Nixon, S., Cousins, C. R., & Cockell, C. (2013). Plausible microbial metabolisms on Mars. *Astronomy & Geophysics*, 54(1), 1.13–1.16.
- Óladóttir, B. A., Larsen, G., & Sigmarsson, O. (2011a). Holocene volcanic activity at Grímsvötn, Bárðarbunga and Kverkfjöll subglacial centres beneath Vatnajökull. *Iceland. Bulletin of Volcanology*, 73(9), 1187–1208. <https://doi.org/10.1007/s00445-011-0461-4>
- Óladóttir, B. A., Larsen, G., Sigmarsson, O., & Devidal, J.-L. (2011b). Provenance of basaltic tephra from Vatnajökull subglacial volcanoes,

- Iceland, as determined by major- and trace-element analyses. *Holocene*, 21(7), 1037–1048. <https://doi.org/10.1177/0959683611400456>
- Ólafsson, M., Torfason, H., & Grönvold, K. (2000). Surface exploration and monitoring of geothermal activity in the Kverkfjöll geothermal area, central Iceland. *World Geothermal Congress, 2000*, 1539–1545.
- Osinski, G. R., Tornabene, L. L., Banerjee, N. R., Cockell, C. S., Flemming, R., Izawa, M. R. M., McCutcheon, J., Parnell, J., Preston, L. J., Pickersgill, A. E., Pontefract, A., Sapers, H. M., & Southam, G. (2013). Impact-generated hydrothermal systems on Earth and Mars. *Icarus*, 224(2), 347–363. <https://doi.org/10.1016/j.icarus.2012.08.030>
- Phillips, R. J., Zuber, M. T., Solomon, S. C., Golombek, M. P., Jakosky, B. M., Banerdt, W. B., Smith, D. E., Williams, R. M., Hynes, B. M., Aharonson, O., & Hauck, S. A. 2nd (2001). Ancient geodynamics and global-scale hydrology on Mars. *Science*, 291(5513), 2587–2591. <https://doi.org/10.1126/science.1058701>
- Pirajno, F., & Van Kranendonk, M. J. (2007). Review of hydrothermal processes and systems on Earth and implications for Martian analogues. *Australian Journal of Earth Sciences*, 52(3), 329–351. <https://doi.org/10.1080/08120090500134571>
- Price, A., Pearson, V. K., Schwensen, S. P., Miot, J., & Olsson-Francis, K. (2018). Nitrate-dependent iron oxidation: A potential Mars metabolism. *Frontiers in Microbiology*, 9, 513. <https://doi.org/10.3389/fmicb.2018.00513>
- Quast, C., Pruesse, E., Yilmaz, P., Gerken, J., Schweer, T., Yarza, P., Peplies, J., & Glöckner, F. O. (2012). The SILVA ribosomal RNA gene database project: Improved data processing and web-based tools. *Nucleic Acids Research*, 41(D1), D590–D596. <https://doi.org/10.1093/nar/gks1219>
- Reysenbach, A. L., Liu, Y., Banta, A. B., Beveridge, T. J., Kirshtein, J. D., Schouten, S., Tivey, M. K., Von Damm, K. L., & Voytek, M. A. (2006). A ubiquitous thermoacidophilic archaeon from deep-sea hydrothermal vents. *Nature*, 442(7101), 444–447.
- Richter, B., Steingrímsson, B., Ólafsson, M., & Karlsdóttir, R. (2010). *Geothermal Surface Exploration in Iceland*. Proceedings World Geothermal Congress 2010, Bali, Indonesia, 25–29 April 2010.
- Rimmer, P. B., Shorttle, O. (2019). Origin of life's building blocks in carbon-and nitrogen-rich surface hydrothermal vents. *Life*, 9, 12. <https://doi.org/10.3390/life9010012>
- Ruff, S. W., & Farmer, J. D. (2016). Silica deposits on Mars with features resembling hot spring biosignatures at El Tatio in Chile. *Nature Communications*, 7, 1–10. <https://doi.org/10.1038/ncomms13554>
- Ruff, S. W., Farmer, J. D., Calvin, W. M., Herkenhoff, K. E., Johnson, J. R., Morris, R. V., Rice, M. S., Arvidson, R. E., Bell, J. F., Christensen, P. R., & Squyres, S. W. (2011). Characteristics, distribution, origin, and significance of opaline silica observed by the Spirit rover in Gusev crater. *Mars. Journal of Geophysical Research: Planets*, 116(E7), E00F23. <https://doi.org/10.1029/2010JE003767>
- Sánchez-Andrea, I., Rodríguez, N., Amils, R., & Sanz, J. L. (2011). Microbial diversity in anaerobic sediments at Rio Tinto, a naturally acidic environment with a high heavy metal content. *Applied and Environment Microbiology*, 77(17), 6085–6093.
- Scanlon, K. E., Head, J. W., Wilson, L., & Marchant, D. R. (2014). Volcano-ice interactions in the Arsia Mons tropical mountain glacier deposits. *Icarus*, 237, 315–339. <https://doi.org/10.1016/j.icarus.2014.04.024>
- Scanlon, K. E., Head, J. W., Wilson, L., & Marchant, D. R. (2015). Volcanism-induced, local wet-based glacial conditions recorded in the Late Amazonian Arsia Mons tropical mountain glacier deposits. *Icarus*, 250, 18–31. <https://doi.org/10.1016/j.icarus.2014.11.016>
- Schmitt, B., Brönnimann, C., Eikenberry, E. F., Gozzo, F., Hörmann, C., Horisberger, R., & Patterson, B. (2003). Mythen detector system. *Nuclear Instruments and Methods in Physics Research Section A: Accelerators, Spectrometers, Detectors and Associated Equipment*, 501(1), 267–272.
- Schloss, P. D., Westcott, S. L., Ryabin, T., Hall, J. R., Hartmann, M., Hollister, E. B., Lesniewski, R. A., Oakley, B. B., Parks, D. H., Robinson, C. J., Sahl, J. W., Stres, B., Thallinger, G. G., Van Horn, D. J., & Weber, C. F. (2009). Introducing mothur: Open-source, platform-independent, community-supported software for describing and comparing microbial communities. *Applied and Environmental Microbiology*, 75(23), 7537.
- Schouten, S., Baas, M., Hopmans, E. C., Reysenbach, A. L., & Damsté, J. S. S. (2008). Tetraether membrane lipids of *Candidatus "Aciduliprofundum boonei"*, a cultivated obligate thermoacidophilic euryarchaeote from deep-sea hydrothermal vents. *Extremophiles*, 12(1), 119–124. <https://doi.org/10.1007/s00792-007-0111-0>
- Schulze-Makuch, D., Dohm, J. M., Fan, C., Fairen, A. G., Rodriguez, J. A. P., Baker, V. R., & Fink, W. (2007). Exploration of hydrothermal targets on Mars. *Icarus*, 189(2), 308–324. <https://doi.org/10.1016/j.icarus.2007.02.007>
- Segura, T. L., Owen, B. T., Anthony, C., & Kevin, Z. (2002). Environmental effects of large impacts on Mars. *Science*, 298(5600), 1977–1980. <https://doi.org/10.1126/science.1073586>
- Sigmarrsson, O., & Steinthórsson, S. (2007). Origin of Icelandic basalts: A review of their petrology and geochemistry. *Journal of Geodynamics*, 43(1), 87–100. <https://doi.org/10.1016/j.jog.2006.09.016>
- Sigvaldason, G. E. (1974). Basalts from the centre of the assumed Icelandic mantle plume. *Journal of Petrology*, 15(3), 497–524. <https://doi.org/10.1093/petrology/15.3.497>
- Skok, J. R., Mustard, J. F., Ehlmann, B. L., Milliken, R. E., & Murchie, S. L. (2010). Silica deposits in the Nili Patera caldera on the Syrtis Major volcanic complex on Mars. *Nature Geoscience*, 3(12), 838–841. <https://doi.org/10.1038/ngeo990>
- Squyres, S. W., Arvidson, R. E., Ruff, S., Gellert, R., Morris, R. V., Ming, D. W., ... McLennan, S. M. (2008). Detection of silica-rich deposits on Mars. *Science*, 320(5879), 1063–1067.
- Stefánsson, A., Keller, N. S., Robin, J. G., Kaasalainen, H., Björnsdóttir, S., Pétursdóttir, S., Jóhannesson, H., & Hreggvidsson, G. O. (2016). Quantifying mixing, boiling, degassing, oxidation and reactivity of thermal waters at Vonarskard, Iceland. *Journal of Volcanology and Geothermal Research*, 309, 53–62. <https://doi.org/10.1016/j.jvolg.2015.10.014>
- Tanaka, K. L., & Scott, D. H. (1987). *Geologic Maps of the Polar Regions of Mars*. US. Geol. Surv., Miscellaneous Investigations (Series Mpa 1-802-C, Scale 1:15,000,000).
- Thór Marteinsson, V., Rúnarsson, Á., Stefánsson, A., Thorsteinsson, T., Jóhannesson, T., Magnússon, S. H., Reynisson, E., Einarsson, B., Wade, N., Morrison, H. G., & Gaidos, E. (2013). Microbial communities in the subglacial waters of the Vatnajökull ice cap, Iceland. *The ISME Journal*, 7(2), 427–437. <https://doi.org/10.1038/ismej.2012.97>
- Van Bodegom, P. M., Scholten, J. C., & Stams, A. J. (2004). Direct inhibition of methanogenesis by ferric iron. *FEMS Microbiology Ecology*, 49(2), 261–268. <https://doi.org/10.1016/j.femsec.2004.03.017>
- Van Kranendonk, M. V., Damer, B. F., Boyd, E., Cady, S., Campbell, K., Czaja, A., Baumgartner, R., Deamer, D. W., Djokic, T., Fiorentini, M., Gangadine, A., Havig, J., Mulikidjanian, A., Ruff, S., & Thordarson, P. (2018). Terrestrial hot springs and the origin of life: implications for the search for life beyond earth. In *Lunar and Planetary Science Conference* (No. 2083, p. 2535).
- Wagner, J., Coupland, P., Browne, H. P., Lawley, T. D., Francis, S. C., & Parkhill, J. (2016). Evaluation of PacBio sequencing for full-length bacterial 16S rRNA gene classification. *BMC Microbiology*, 16(1), 1–17.
- Wallwork, K. S., Kennedy, B. J., & Wang, D. (2007). The high resolution powder diffraction beamline for the Australian Synchrotron. In *AIP Conference Proceedings* (Vol. 879, No. 1, pp. 879–882). American Institute of Physics.
- Westall, F., Foucher, F., Bost, N., Bertrand, M., Loizeau, D., Vago, J. L., Kmínek, G., Gaboyer, F., Campbell, K. A., Bréhéret, J.-G., Gautret, P., & Cockell, C. S. (2015). Biosignatures on Mars: What, where, and

- how? Implications for the search for martian life. *Astrobiology*, 15(11), 259–293. <https://doi.org/10.1089/ast.2015.1374>
- Wordsworth, R. D. (2016). The climate of Early Mars. *Annual Review of Earth and Planetary Sciences*, 44, 381–408. <https://doi.org/10.1146/annurev-earth-060115-012355>
- Zerkle, A. L., House, C. H., & Brantley, S. L. (2005). Biochemical signatures through time as inferred from whole microbial genomes. *American Journal of Science*, 305, 467–502. <https://doi.org/10.2475/ajs.305.6-8.467>
- Zerkle, A. L., Jones, D. S., Farquhar, J., & Macalady, J. L. (2016). Sulfur isotope values in the sulfidic Frasassi cave system, central Italy: A case study of a chemolithotrophic S-based ecosystem. *Geochimica et Cosmochimica Acta*, 173, 373–386. <https://doi.org/10.1016/j.gca.2015.10.028>

SUPPORTING INFORMATION

Additional supporting information may be found online in the Supporting Information section.

How to cite this article: Moreras-Marti A, Fox-Powell M, Zerkle AL, et al. Volcanic controls on the microbial habitability of Mars-analogue hydrothermal environments. *Geobiology*. 2021;00:1–21. <https://doi.org/10.1111/gbi.12459>